Heat Transfer and Latent Heat Storage in Inorganic Molten Salts for Concentrating Solar Power Plants

Final Report

Report Number: DOE-GO18148

Phase I & 2

Prepared by

Anoop Mathur (Terrafore Inc.)
Rajan Kasetty (Terrafore Inc.)
Prof. Javier Garay (UCR)
Prof. Chris Dames (UCR)
Corey Hardin (UCR)
Mehrnoush Zare (UCR)
Mike McDowell (PWR)
Gyan Hajela (PWR)
Dr. Subbarao Surampudi (JPL)
Dr. Andrew Kindler (JPL)
Dr. Parthasarathy Shakkottai (JPL)
Dr. H. Venkatasetty (Setty Enterprises)

May 14, 2012

Submitted to
U.S. Department Of Energy
Contract: DE-FG36-08GO18148

Contact:
Anoop Mathur
Terrafore, Inc.
100 South 5th St, Suite 1900, Minneapolis, MN 55402
anoop.mathur@terrafore.com

.

Table of Contents

Appendices

To

Sections

Appendix 1
Eutectic Phase Diagrams

By
Mehrnoush Zare

Phase Diagram and Heat of Fusion Calculations

In Table 3, we list the heat of fusion of eutectic salt mixtures that are major components. The procedure described below is used to calculate the heat of fusion and freezing point depression for the salt mixture consisting of the major and minor components. Appendix C shows the procedure for calculating the heat of fusion and freezing point depression for a few selected salt mixtures. The phase diagrams for some salt systems are available in literature (ref : Tohoku database). Appendix D shows some of the phase diagrams and calculation procedure.

In order to obtain the maximum mass percentage of the first solidified salt which can be released during the solidification process at any temperature range, one can take advantage of the lever rule. This can also be used to determine the amount of latent heat of fusion by multiplying the percentage of solidification with the latent heat of the solidified salt, and adding the sensible heat due to the freezing point depression to the final solidification point.

The best binary would have a small liquidus slope at the solute rich- side of the diagram. This can be determined by simply determining the slope from the A-B diagram. We introduce a term called *effectivity index* to compare different salt systems with each other:

$$effectivity\ index = \frac{effective\ latent\ heat}{slope\ of\ the\ liquidus\ line\ in\ phase\ diagram}$$

Therefore the higher the effectivity index, the better the salt mixture as a PCM, since it stores and releases more latent heat and its liquidus slope is relatively lower.

Another approach would be to calculate the freezing point depression of the solvent A by the addition of the solute B. Freezing-point depression describes the phenomenon that the freezing point of a liquid (a solvent) is depressed when another compound is added, meaning that a solution has a lower freezing point than a pure solvent. This happens whenever a solute is added to a pure solvent. The freezing point depression is a colligative property, which means that it is dependent on the presence of dissolved particles and their number, but not their identity. It is an effect of the dilution of the solvent in the presence of a solute. It is a phenomenon that happens for all solutes in all solutions, even in ideal solutions, and does not depend on any specific solute-solvent interactions.

The extent of freezing-point depression can be calculated by applying Clausius-Clapeyron relation and Raoult's law together with the assumption of the non-solubility of the solute in the solid solvent. The equation is $\Delta T = R (T_m)^2 X_n / L$, where X_n is mole fraction and L is the heat of fusion. This will give us a quantitative selection parameter that approximately follows the calculated slope values.

The equation can also be shown as $\Delta T = K_c X_n$, where $K_c = R (T_m)^2/L$ is called the cryoscopic constant. The technique for determining the molecular weight of a solute by dissolving a known quantity of it in a solvent and recording the amount by which the freezing point of the solvent drops, is called cryoscopy.

Therefore the phase diagram calculations were done for each 10 systems in table 1. First the amount of molar solidification percentage was calculated when cooling down from 350°C to 270°C. Then the same thing was calculated while cooling down from 290°C to 270°C in order to obtain the amount of solidification with approximately 20°C temperature depression. Mass percentage of solidification was determined using the below equation:

If the initial composition of the salt is xA0 and xB0, then the composition of the salt after mass% of solidification is:

$$Mass\% = \frac{x_A \times mW_A}{x_A \times mW_A + x_B \times mW_B}$$

Where x_A and x_B are the molar percentages of A and B and $mW_A and\ mW_B$ are molar masses of A and B respectively. The effective latent heat, slope of the liquidus line, effectivity index, cryoscopic constant and sensible heat release were also calculated for each system.

For the ternary systems one can assume a binary eutectic composition as a single salt phase with the melting temperature of the eutectic point and the latent heat obtained by the rule of mixture. By adding a small amount of the third salt, the amount of temperature depression will be calculated like the binary systems from the equation: $\Delta T = R (T_m)^2 X_n / L$

Therefore, for the ternary systems melting temperature will be the eutectic temperature for the major binary salts and latent heat is obtained by the rule of mixture at the eutectic composition. The cryoscopic constant was also calculated for the ternary systems.

Viscosity of the semi-solid salt mixtures

The rheological behavior of partially solidified salt mixtures to be used in solar power plants is our interest. It is known that in the early stages of solidification, shrinkage is compensated for the simultaneous movement of liquid and solid. This can be called mass feeding. At later stages of solidification the growing dendrites form a continuous skeleton within the liquid-solid zone. As cooling continues, this skeleton is subjected to strain from thermal contraction and this strain can be highly localized. Within local regions of high strain, bonds between dendrites and dendrite arms are broken and dendrites separate.

Vigorous agitation of a molten salt mixture however postpones the formation of a continuous solid network to much higher fraction solid. With this agitation we can make the mixture to behave as thixotropic slurry to fractions of solid up to 50%. Being thixotropic means to become as less viscose as the fluid itself when stirred or shaken and returning to a semi-solid state when allowed to stand.

Apparent viscosity of slurries increases with increasing solid concentration. Therefore solid fraction plays an important role in semi-solid. Cooling rate is another important factor. By decreasing temperature, the viscosity of the semi-solid will increase faster. Dendrite network will be formed faster in this situation in absence of a stirring system.

In the presence of the stirring system the below equation in introduced for simple Newtonian fluids:

$$Viscosity = \frac{Shear\ Stress}{Shear\ Rate}$$

In rheocasting or simply stirring the melt, there is a fixed amount of force applied, therefore when shear rate increases, the viscosity decreases. This is significant in the current research for the ease of pumping the semi-solid salt mixture through the heat exchanger tubes and pumping the high fraction semi-solid out of the heat exchanger tubes to the main tank.

Collected data for a variety of dispersed Newtonian suspensions are shown in figure 1. As it can be seen the apparent viscosity between "0.4 to 0.6" of solid fraction, increases to very high values. When plotted as relative viscosity versus fraction solid, all the data fall on the same general curve regardless of material. If we assume that our solid particles in semi-solid salt mixture are also spherical in shape with the range of diameter between 0.099 to 435 Microns, as it is for the particles in the figure 4, we can use the same values to estimate a bulk figure for the changing of the viscosity in salt mixture by solid fraction.

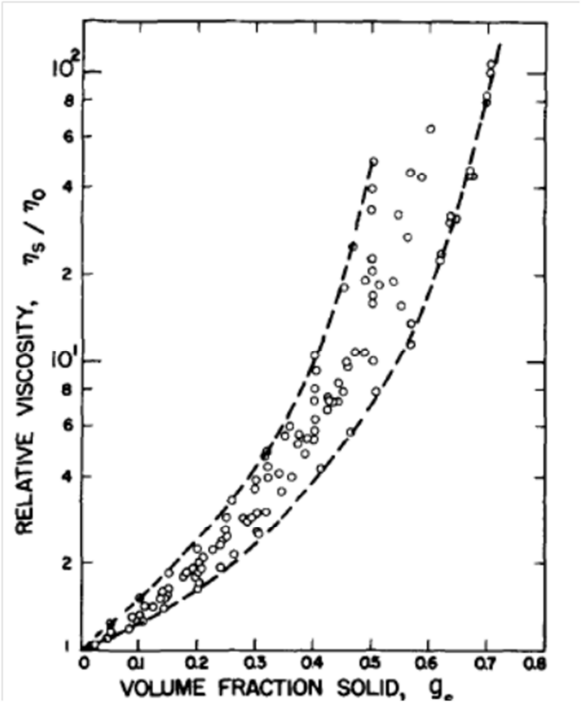

Figure 1. Collected viscosity data of dispersed suspensions of uniform spherical particles. The particle materials included polystyrene, rubber latex, glass, and methyl methacrylate. η_s is the viscosity of the slurry while η_o is the viscosity of the suspending medium [D.B. Spencer, et al, MMT, vol.3 (1973)]

Temperature change is also another factor to be considered. Let us assume a binary salt system A-B which by decreasing the temperature below the liquidus line, salt B starts to solidify first. Because of the temperature depression, there will be an increase on the viscosity of the liquid phase itself ignoring the solid fraction. So there will be a relationship between temperature and viscosity. Also by increasing the solid particles there will be a relationship between solid fraction and viscosity, which is indicated in figure 1. Because the solid fraction is also related to temperature according to the binary system's phase diagram, therefore by combining these two relationships, we can better determine the viscosity change of the salt mixture during the solidification.

It is also to be mentioned that the liquid phase is a molten salt mixture. Therefore by decreasing the temperature the percentage of the saluted salt is decreasing in the liquid phase, and this will cause a

deviation from the viscosity data in the liquid phase. So for accurate viscosity data experimental methods seem to be necessary. However we could estimate the change of the viscosity by temperature decrease and solute increase by doing some simple calculations. These calculations are done for each binary system below, and the results are compared between for systems at the end. The relative viscosity data in figure 4 assumed to be increasing exponentially by increasing the solute as solid particles, as it can be seen in the below equation:

$$\eta = \eta_o \exp(s\%) \ [CP]$$

Measuring viscosity at or near freezing or melting temperature is challenging. Figure 2 shows the viscosity of sodium nitrate salt near melting temperatures (300 to 308 C). These measurements were at conducted at NREL by Dr. Anne Starace.

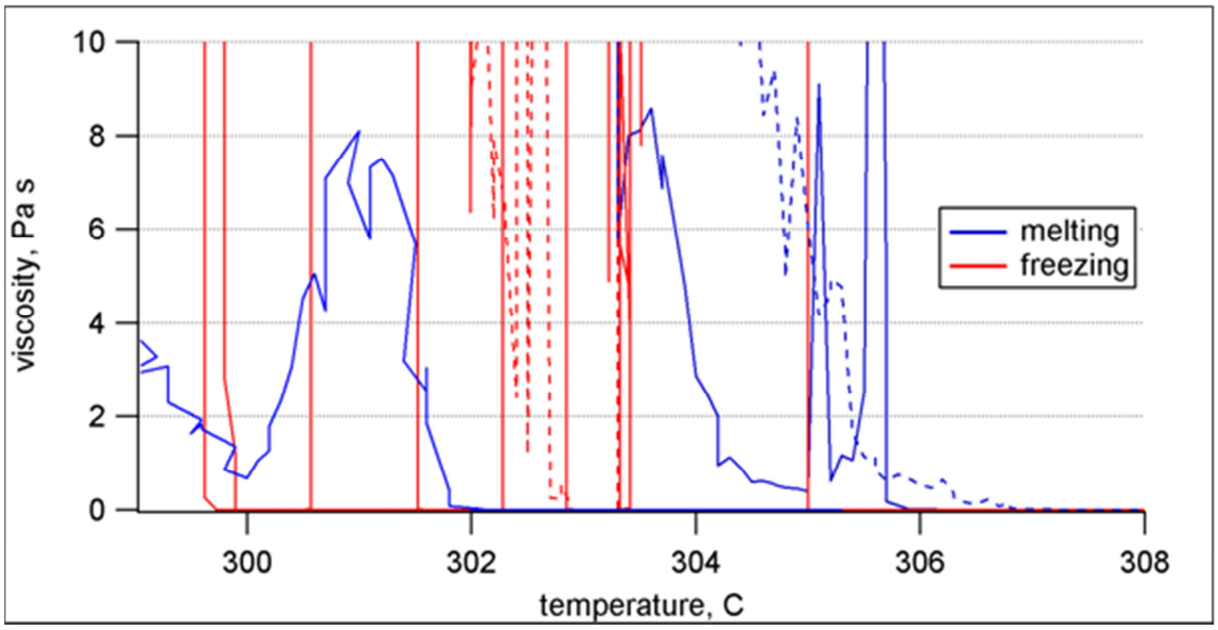

Figure 2. Measurement of viscosity near freezing and melting temperatures for NaNO3
(courtesy Dr. Anne Starace Scientist NREL)

Considerations in Selecting Salt Mixtures

Dr. H. Venkatasetty

Nucleation and Crystallization

Super-cooling of melts, which precludes crystallization and heat release, is one of the problems in the selection of suitable thermal energy storage materials. Our experience shows that the phase–change processes (heating and cooling) do not occur instantaneously as expected. However, the process can be hastened by using suitable nucleating agents. We believe that in large storage systems we are considering for this project, it becomes even more important to identify suitable nucleating agents and conduct preliminary experiments.

Although this problem is well documented in the literature, not much is known on promising nucleating agents for accelerating nucleation and crystal growth in phase-change materials. An understanding of the process involved has direct influence on the heat transfer rate as well as the removal of solidified material from the heat transfer surface. Ideally, the best nucleating agent for salt mixture(s) considered should have similar crystal structure and chemically inert and have high melting point. Understanding the interrelationship between the critical size of the cluster (nucleating agent) and the energy of activation for crystal formation is helpful (1, 2).

Therefore, it is desirable to identify a small number of promising salts that can be studied as suitable and compatible nucleating agents to the eutectic mixtures. These materials should be potentially inert at the temperatures of interest. A few are being recommended as potential materials for early experimentation in the laboratory. Some of these are:

Calcium nitrate Ca (NO3) 2 which has high melting point of 561 C, has cubic crystalline structure, but hygroscopic. Small amount of anhydrous reagent grade salt can be obtained. Another compound is Tungsten oxide (WO3) with high melting point of 14730C and has orthorhombic structure. Low cost Potassium carbonate K2 CO3 with the melting point of 8910C with monoclinic structure is a candidate material. The disadvantage of these materials is that they are not inert and they can interact with the one or more of the components of the eutectic.

Therefore, two inert compounds are suggested: One of them is Titanium Oxide (TiO2).

It has very high melting point (1840°C) and has low thermal expansion coefficient and has been used in certain glass ceramics as a nucleating agent.

Another potential nucleating agent is Zirconia (ZrO2)- a refractory material that has a very high melting point of 2700°C and low thermal expansion coefficient.

Corrosion Rates

Table 4 lists some of the corrosion rates with salts and containment.

Table 4. Corrosion Data for selected components of chemicals in salt mixtures for some container materials

Chemical in the eutectic mixture	***Container Materials***		
	Cast Iron	***Mild Steel***	***Stainless steels***
NaOH	***> 50 Mil/year****	***> 50 Mil/year***	***< 2 to <20 Mil/year***
NaCl			***20 to 50 Mil/year***
$NaNO_3$ SS302) ***		***< 2 Mil/year ****	***> 50 Mil/year (SS 347,***
Na_2SO_4			***> 50 Mil/year***
Na_2CO_3		***> 50 Mil/year*****	
KOH			***> 50 Mil/year***
KNO_3			***< 2 Mil/year***

*** stress, @300C **decarburize**

****** @ 450C with SS 347 has 0.08 % carbon, 18% Cr, 11% Ni and 0.8% Nb. Widely used SS 304 & SS 316 have 0.08% carbon, 19%Cr for 304 and 17%Cr for 316, and 12% Ni for 304 and 11% Ni for 316 and 2.5% Mo for 316.***

Majority of eutectic mixtures with useful melting points in the range of 275 to 350 C, and relatively high heat of fusion, contain anions such as nitrates, hydroxides, sulfates and carbonates with cations of mostly sodium and in some cases potassium partly due to availability and cost. These salts, even in moderately pure state and particularly of commercial grade, contain small amounts of impurities such as chlorides (~ 0.001 to .005%), sulfates (≤ .003%), carbonates (≤ 1%) and Fe (≤ 0.001%) that aggravate corrosion to common container materials. Potentially attractive storage container materials are mild-steels, carbon-steels and cast-irons. Mild-steels contain 0.15 to 0.3% Carbon. Carbon-steels contain up to ~ 2 % carbon and may also contain other elements, such as Silicon (maximum0.6%), Copper (up to 0.6%) and Manganese (up to 1.65%). Cast-irons are Fe-C alloys containing 2 to 4% Carbon. (1). Stainless steels such as 304 and other types contain carbon, chromium and nickel and other metals. For example, Stainless steel 304 has 0.08% carbon, 19% Cr and 10% Ni, stainless steel 304L has 0.03% Carbon, 19%Cr and 10%Ni and Stainless steel 316 has 0.08% Carbon, 17%Cr, 12%Ni and 2.5% Mo. Stainless steel 347 has 0.08%Carbon, 18% Cr, 11%Ni and 0.8%Nb (1

Physical stability and the composition of the container material in contact with the molten salt mixtures are affected by the corrosive properties of molten salt component of the eutectics and some specific impurities present in them by two types of corrosion processes (2). These are chemical corrosion and electrochemical corrosion. The corrosion data for selected container materials in presence of some common molten salt components are listed in Table 4 (3).

Table 6 shows that pressure has little effect on the properties of molten NaNO3 and NaOH. Details of these calculations are shown in Appendix E.

Selected Properties of NaNO3 mixtures

Properties of NaNO3, NaO3					
Property	**Units**	**NaNO3**	**NaOH**	**Eutectic**	**Dilute Eutectic**
Molecular Weight		85	40	71.5	83
Melting Point	Deg C	310	318		
Liq Density	kg/m3	1910	1785	1929	1930
Solid Density	kg/m3				
Heat of Fusion	kCal/mole	3.52	1.52	2.92	3.475
Viscosity	cP	2.89	5.15	3.33	2.9
Heat Capacity	kJ/kg-K	1.84	2.0724		
Thermal Conductivity	W/m-K	0.57	0.8302		
Prandtl Number		9.3	12.9		

Properties of NaNO3 as function of pressure			
Property	**Units**	**P= 1 atm**	**P= 100 atm**
Density	kg/m3	1910	1913
Viscosity	cP	3.062	3.068
Thermal Conductivity	W/m-K	0.57	0.5702
Heat Capacity	kJ/kg-K	1.84	1.832
Isothermal Compressibility	cm2/dyne	17.8 e-12	
velocity of sound	m/s	1704	

Appendix 2 .
Selection of 'Salt-Phobic' Coatings

This section discusses the methods used to select 'anti-stick' coating materials to be used on heat exchangers for storing thermal energy as latent heat of fusion in mixtures of inorganic salts. To enhance heat transfer from freezing salt mixtures heat exchanger tubes are coated so that the force of molten salt at near freezing point pumped from a tank and flowing past the tubes can remove the solid material. The resulting solid slurry is returned to the tank. The heat transfer coefficient is expected to be much higher than passive solidification on tubes.

Statement of the Heat Transfer Problem and Approach to Solution

A major drawback of using phase change molten salt materials is their poor thermal conductivity and the fact that clumping occurs during freezing that sticks to the walls of the storage tank and heat exchanger surfaces. Using our storage media of dilute eutectic would alleviate this problem. As discussed in report on Salt Selection, when a dilute eutectic mixture, such as with a large fraction of NaNO3 in a NaNO3-NaOH mixture, freezes, there is always liquid around the freezing NaNO3. The freezing material is 'mushy' and even though highly viscous, can be pumped to an external heat exchanger. (Note: This is similar to what happens in an ice-cream plant. In these plants, additives such as polysaccharides are added to the ice cream so that it can be easily pumped.)

In addition to taking advantage of the liquid in equilibrium in freezing solid, we are investigating coating materials that can apply to heat exchanger tubes. The coating materials are referred to as 'anti-stick' because the freezing material can be easily removed from it. This is similar to 'Teflon' used in common kitchenware. The coating material should be 'non-stick' to freezing material and have high thermal conductivity. In this report we present results with coating materials such as graphite, metallic nitrides and carbides, and high temperature polymers (such as imides, poly benzo-oxy imidazole). These coatings are deposited on heat exchanger tubes.

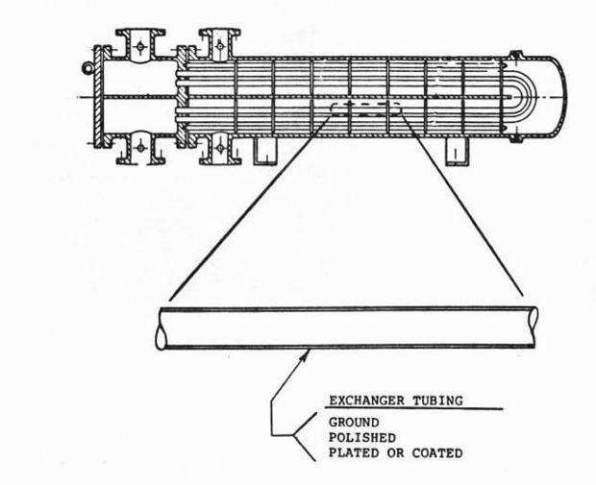

Figure 1. Low adhesion surfaces and shell and tube heat exchangers offer

There are many types of heat exchangers used in the industry for transferring heat during phase change from liquid to solid. Some of the active (not passive) heat exchange designs include shell and coated tubes; others use mechanical scrapers, ultrasonic vibrations or flexing to free the tubes of freezing salts. Three methods show promise:

- use of coated heat exchanger tubes (researched in this project)
- encapsulation of salt in suitable shell material
- direct contact of salt with heat transfer medium such as bubbling water through molten salt.

Our preliminary analysis, based on past research indicates that the shell and tube type of heat exchangers, with the salt on the shell side and the two-phase steam water inside the tube can potentially be successful

when discharging heat from the PCM melt. Furthermore, since this is a commonly used design in the industry it is also the most economical to use.

In addition to the two methods – dilute eutectic mixture and 'anti-stick' coating - , we will investigate a third way to further improve the flow properties and improve the conductivity. We are investigating using additives such as graphite, Nano-carbonaceous materials, and ionic liquids. . We propose these materials because of their high thermal stability, and chemical stability, good heat transfer properties and good non-wetting characteristics with molten salts. We will present the results of this later in another report.

Candidate Coatings

Our approach to selecting and testing coatings consisted of the following steps:

- Use scientific expertise to select a subset of coating candidates
- Use qualitative *dip-test* method to screen and select at least three candidate coatings
- Examine the interface between the solid and substrate using Scanning Electron Microscopy and Optical Microscopy to characterize the morphology of freezing crystals
- Procure tubes coated with the selected coatings and test them on a 'flow rig' specifically designed to freeze salt on the tubes and remove it by using hydrodynamic forces from a flowing salt.

The results from these steps are described below. The tests provide a comparative and qualitative evaluation of selected coatings. A few coatings have been tested. We are discussing with coating vendors for providing samples for a few other coatings. We will continue these tests in Phase II in parallel with the heat exchanger tests planned.

Selection Criteria of Coatings

The strategy for choosing a coating was relatively straight forward. We surveyed the coatings available, and chose those that could handle 4000C or greater. Once we had a collection of such coatings, we further selected from this group coatings which had desirable surface properties. These properties were low roughness, and a hydrophobic nature. A hydrophobic surface is considered desirable because it has a low surface energy. This means that intermolecular attraction between the surface and a crystallite will be limited. As a result "stickiness" of the crystallite should be should be minimized.

A smooth surface is also highly advantageous for two reasons. First of all, lock and key binding of the crystallite to the surface is minimized, second reduced contact surface area minimizes the effect of the intermolecular forces. In effect, the smooth surface enhances its already hydrophobic nature. Appendix A further describes a scientific basis for selecting coatings.

Table 1 is an initial selection of coatings based on the collective scientific thought process which is discussed in the following paragraphs.

Generally speaking, the best coatings are created by physical vapor deposition (PVD), chemical vapor deposition (CVD), and other surface modifying processes carried out in vacuum systems. These coatings are thin, and smooth. Because they are thin, it is expected that heat transfer through them will not be significantly inhibited. The benefit of a smooth coating has already been addressed.

We did not consider using any coating that is applied by flame spraying or similar process because the coatings tend to be porous. This is in line with our desire to maintain a smooth surface. For this reason we did not use Alumina, Chromium Carbide, and Tungsten Carbide.

Boron Nitride was not tested in our first set of experiments. Boron Nitride is generally used in applications were it s not firmly bonded to the surface. For this reason, the common coatings do not firmly adhere to the substrate. An example is its use as a mold release agent. Additionally, Boron Nitride in its most common (hexagonal) form is quite soft. These properties make it less than ideal despite the fact that it is an extremely hydrophobic material. A less common form of Boron Nitride is the cubic variety. In this form, its crystal structure is diamond like, and it is very hard. This form can be applied so that it is very thin. The cubic form is probably suitable for our application and will be a candidate for future experiments once we find a vendor who will apply this coating.

Titanium Carbide is known to have non stick properties in molten salt baths. It surface is extremely smooth and can be made quite thin. It is an excellent candidate.

Titanium Nitride and Chromium Nitride can both be applied in a very thin smooth layer. Both are also known to be hydrophobic. The vendor also supplies a more hydrophobic silicate based coating that can be applied over either nitride and is also extremely thin. This overcoat is said to bond more effectively to the nitride surface than the steel substrate alone. It is subject to a lower maximum temperature limit.

Porcelain is very smooth and would be expected to be low cost because it is a commercial product with a variety of applications. It is not as thin as coats applied using PVD or CVD. It is also not quite as hydrophobic because it contains a substantial amount of glass.

Diamond-like coatings are thin, hydrophobic, and very hard. They are potentially ideal candidates. Cost was a concern, but one type is actually used to coat razor blades. We plan to look into whether the type of diamond like coating we would need is equally inexpensive for future experiments.

Two proprietary coatings of unknown composition may also be very suitable. These are Cerablak and FGI-400HR. The latter has been used on heat exchangers. Coated samples may be available pending special arrangements.

Table 1 CANDIDATE COATINGS

*Indicates the material was tested in this reporting period

COATING	SOURCE	COMMENTS	MAX TEMP	HYDROPHOBIC	SURFACE ROUGHNESS
*Mild Steel		CONTROL	N/A	No	Fine Sanding
*Porcelain SH502	Ferro			Somewhat	Very Smooth
*Titanium Carbide on graphite Titanium Carbide on Steel	Solar Atmospheres Ultramet and others	Temperature limited by graphite substrate and presence of air CVD coating on steel also possible	>400	Yes	Very Smooth
*Titanium Nitride	BryCoat	PVD coating	600^{0}C in air	Yes	Smooth
*Chromium Nitride	BryCoat	"	1050^{0}C	Yes	Smooth
*Brycoat HTS over *Titanium Nitride	Brycoat	Proprietary silicate based overcoat	400^{0}C	Yes	Smooth
*Brycoat HTS over *Chromium Nitride	Brycoat	"	400^{0}C	Yes	Smooth
Cubic Boron Nitride (Diamond Like)	Ceratizit	PVD	2973^{0}C	Yes	Smooth
Alumina	Brycoat (and others)	Flame sprayed	1700^{0}C	No	Porous when flame sprayed
Chromium Carbide	Pacific Particulate Materials among others	There are several chromium carbides with different melting points	1250^{0}C - 1895^{0}C	Probably	Porous when flame sprayed
Tungsten Carbide	CCI (Canada)	Flame sprayed	2870^{0}C	Probably	Porous when flame sprayed
FGI-400HR Ceramic Thermal Transfer Coating	FGI International	Used on heat exchangers	980^{0}C	No data yet	No Data yet
Diamond like Carbon	Morgan Advanced Ceramics	Ion Beam and RF plasma deposition	1200^{0}C	Yes	Smooth
Cerablak	Applied Thin Films Inc.	No data	1400^{0}C	Yes	Smooth

Dip Testing Method for Selecting the Coatings

The test we devised is intended as a preliminary, rapid screening test. The idea is to determine if crystallites formed in the molten salt were likely to stick to the surface of the heat exchanger. The test as devised does not duplicate all the conditions within the molten flow loop. As a result, the screening tests will not necessarily duplicate what will be seen in the field. Despite this limitation, it should be able to allow the qualitative comparison of one coating to the other. In certain respects, the test as designed represents a more severe test of crystallite adhesion/accumulation than might be expected in actual operation.

For the purpose of the test, a furnace is equipped (Fig. 3 and Fig. 4) with a stainless steel pot to contain the salt. In the pot are a stirrer and thermocouple. The stirrer is driven by an air motor which can be set to spin very slowly. The stirrer passes through the wall of the furnace through a stainless steel sleeve. This was necessary to eliminate the grinding off of firebrick insulation by the rotating shaft. The thermocouple is connected to a digital temperature controller that replaces the older malfunctioning analog temperature controller originally built into the furnace. The new controller is more reliable, accurate, and easy to read.

The furnace is also provided with an Argon gas port. The purpose is to prevent oxidation of samples where this is an issue and to insure that the molten salt is not affected by CO_2. CO_2 is an issue when the salt contains NaOH. The NaOH can react with the CO_2 to form carbonates, thus changing the melt composition.

In order to evaluate the performance of different coatings we used a "dip" test. This test was conducted in the following manner.

First, the salt is prepared. We used a proprietary binary salt mixture with a dilute eutectic melting about 300^0C. The salt is placed in a 316 stainless steel container. The thermocouple and stirrer are temporarily suspended above the salt. The Argon is turned on and the furnace is closed. The temperature controller is set to 500^0C. This high temperature is needed because the two components are not mixed initially and the salt melting point is higher. Once the melting has begun, the stirrer and thermocouple is lowered into the salt bath. When the bath is completely liquefied, the stirrer is turned on, and the temperature is lowered to 400^0C. Now that the binary mixture is completely mixed, it remains liquid at a lower temperature. The sample is lowered into the bath suspended on a stainless steel wire. After the sample is immersed, the temperature controller is set to 250^0C. The door of the furnace is now cracked open to allow for cooling. When the solution cools to the point that it is full of crystallites, but not fully solidified, the sample is withdrawn. Generally, this occurs at about 300^0C. At this time the sample is briefly inspected to determine if some crystallites are present. As the sample cools off, more crystals form. The former type of crystal sticks out of the surface. The ones formed as a result of cooling in air are relatively flat. They are formed from the adherent film of salt that is liquid at the time of sample withdrawal.

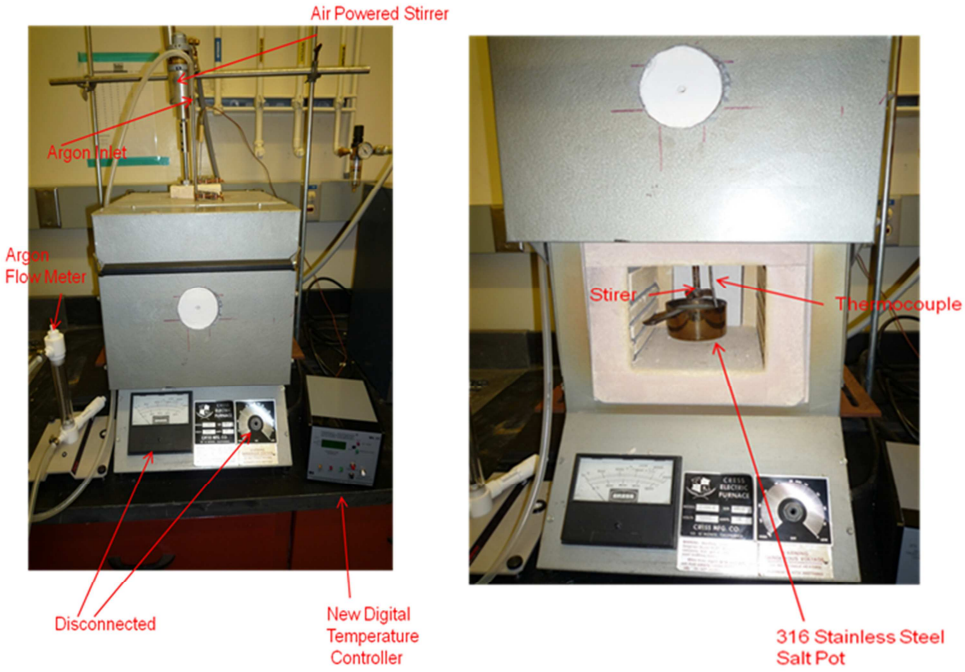

Figures 3 & 4. Dip Test Furnace

Results of Dip Tests

Samples were not characterized quantitatively as to smoothness, but all the samples were very smooth with the possible exception of the mild steel control. This sample was sanded and had obvious markings. The first 3 samples in Table 2 below were of various sizes, the ones after were standardized to 2 cm x 2 cm. The mild steel coupon was prepared under Argon gas blanket to prevent oxidation. The porcelain and Titanium Carbide samples were prepared in air before it was recognized that the bath could degrade as the result of a reaction between NaOH and CO_2. The remaining samples were prepared from a new bath and under an Argon blanket.

The samples were checked for crystallite adhesion when cool. We were looking for very large differences in adhesion so we employed a very simple test. We scraped the surface of the sample with a finger nail. If a crystal could not be removed this way, we considered the surface unsuitable. Those samples were crystals could be removed in this manner were classified as mild or moderate adhesion. Photographs of most of the samples are shown below with explanations. For TiN and CrN (without Brycoat HTS), the adhesion declined after several days.

Table 2. Qualitative Evaluation of Coatings

Material	Adhesion
Mild Steel	Strong
Ferro SH502 Porcelain on Steel	Strong
Solar Atmospheres TiC on Graphite	Mild ***
Brycoat TiN on Mild Steel	Moderate ***
Brycoat CrN on Mild Steel	Mild/Moderate Presumed Surface Damage
Brycoat HTS over Brycoat TiN on mild steel	Strong
Brycoat HTS over Brycoat CrN on mild steel	Strong

***Recommended for Further Testing

Discussion of Results

The sample below shown in Fig. 5 is mild steel with no coating. The bottom accumulation is caused by surface tension effects. Liquid accumulates there during cooling and then freezes. The top accumulation is the liquid line. This sample was tall enough to protrude beyond the liquid level. Crystal accumulation between those lines formed in the pot. The very flat crystals are generated from the liquid film that remained on the sample when it was removed from the pot. All of these crystals were strongly attached.

Figure 5. Photograph of salt on uncoated mild steel surface

The porcelain sample below (Figures 6 & 7) was much smaller. It did not stick out of the melt. The crystals stuck on to the porcelain very strongly despite the shiny surface of the material. This material is

only somewhat hydrophobic, and it might be getting etched by the NaOH. It does not appear to be a candidate choice.

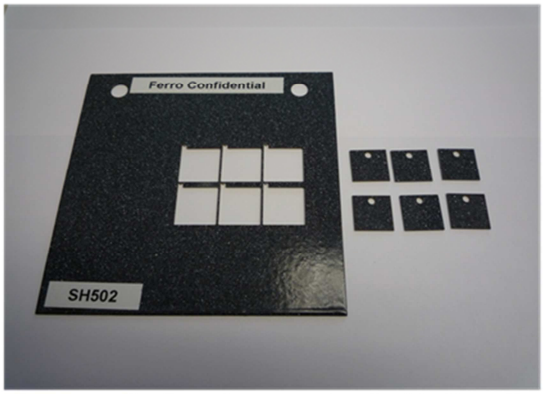

Coupon Before Immersion in Molten Salt

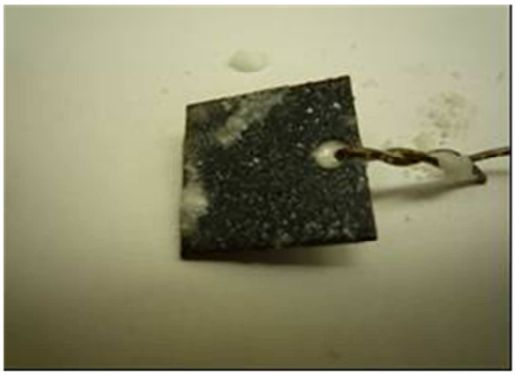

Coupon After Immersion

Figures 6 & 7. Ferro SH 502 Porcelain

The TiC shown in Figures 8 & 9 is grown in situ on a graphite substrate. It is a mirror finish. This is shown by the reflection of a paper clip on to the surface.

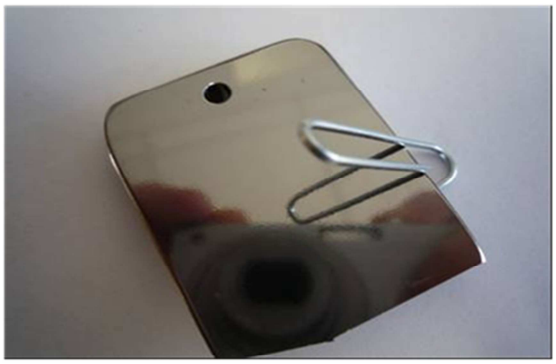

Coupon Before Immersion

Cross Section Showing Graphite Substrate

Figures.

Figures 8 & 9. Photographs of TiC coupon before immersion

The crystal formed on this surface were easy to remove. Figure 10 shows a patch that peeled off by using fingernail pressure. The very smooth deposit suggests that most crystals did not attach while the sample was immersed in the salt. The crystals showing are the type associated with the liquid film that remains o the sample after it is removed from the bath.

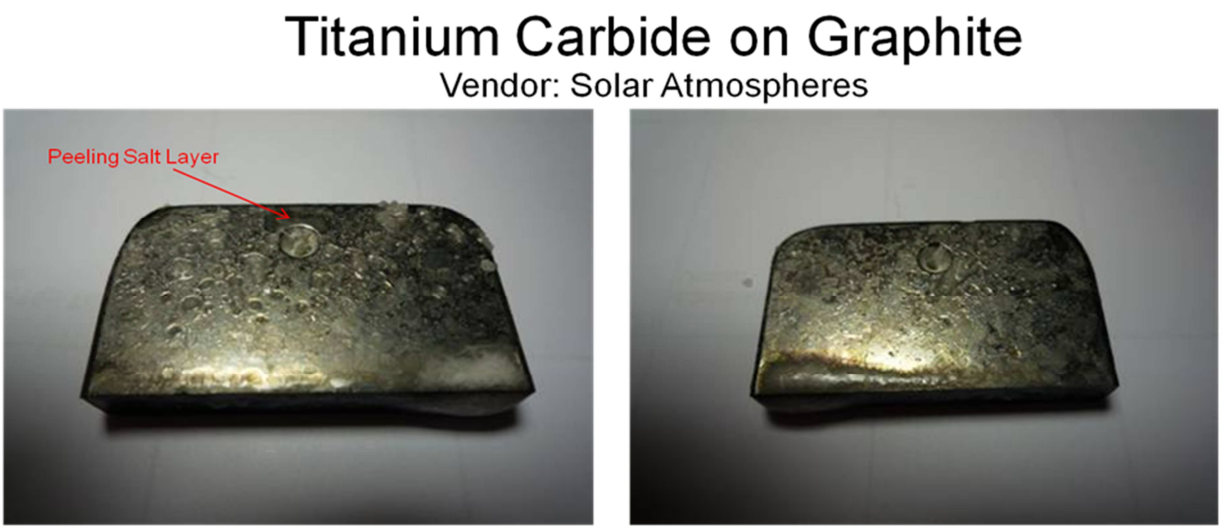

Figures. 10 &11. TiC on Graphite samples

The TiN samples shown in Figure 12 and Figure 13 below are before and after photographs respectively. The surface of the TiN was very smooth, although it was not mirror like. The salt did not stick very strongly to this surface. The photo in Figure 13 (right) shows a small area where the salt peeled off as a result of applying fingernail pressure. After a few days storage in air, the salt came off more easily. The surface did not appear harmed in any way from salt exposure.

Figures 12 & 13. Photographs of TiN on Steel

The CrN samples both before and after are shown in Fig. 14 and 15. The adhesion to this surface was a bit less than the TiN but it was obvious that the sample was damaged in some way because of the discoloration after treatment.

Figure 14 & 15. Photographs of Chromium Nitride coating

Both of the same types of samples were also coated with Brycoat HTS. This silicate based coating is extremely hydrophobic. The coating is not good above 400^0C normally, but we chose to try it anyway because the temperature limit was for exposure to air and because our operating temperature would normally be lower. Our system was more or less free of air so it seemed worth a try. The coating degraded and changed color in patches. Our salt stuck to it very strongly. This proved not to be a good candidate for further screening.

We will continue to test and screen more coating samples in Phase II. The next section describes and discusses the results from the scanning electron microscopy of some of these *dip-coated* samples.

Interface Properties during Freezing of Salt on Coated Tubes

Scanning Electron Microscopy images and discussion for different coatings

Samples from dip tests in salt with the dilute eutectic composition of NaNO3 and NaOH, described earlier, were observed in a Scanning Electron Microscope (SEM) to study the interface properties between the salt and metal surface.

All samples are properly prepared and polished in order to minimize the damage to the surface salt layer, and are coated by Au-Pd to become conductive for SEM microscopy.

The aim of this study is first to measure the thickness of the surface salt layer accurately to compare the different coatings and next to study the surface morphology. The thickness can give us a value for

measuring the stickiness of a certain salt composition to a certain surface and the morphology will provide the types of crystals adhering to the surface.

Figures 16 to 20 show the images of scanning electron microscopy for five different samples: mild steel without coating, mild steel with Porcelain coating, mild steel with CrN coating, mild steel with TiN coating, and graphite with TiC coating in two magnifications.

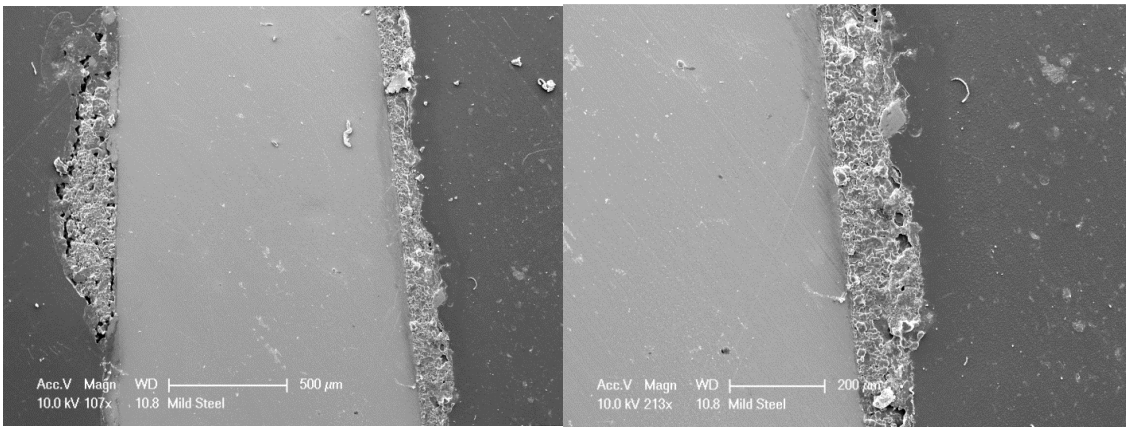

Fig 16 SEM image of the mild steel dipped into the $NaNo_3$(98%)-NaOH(2%) molten salt. The solidified salt layer can be seen in two different magnifications.

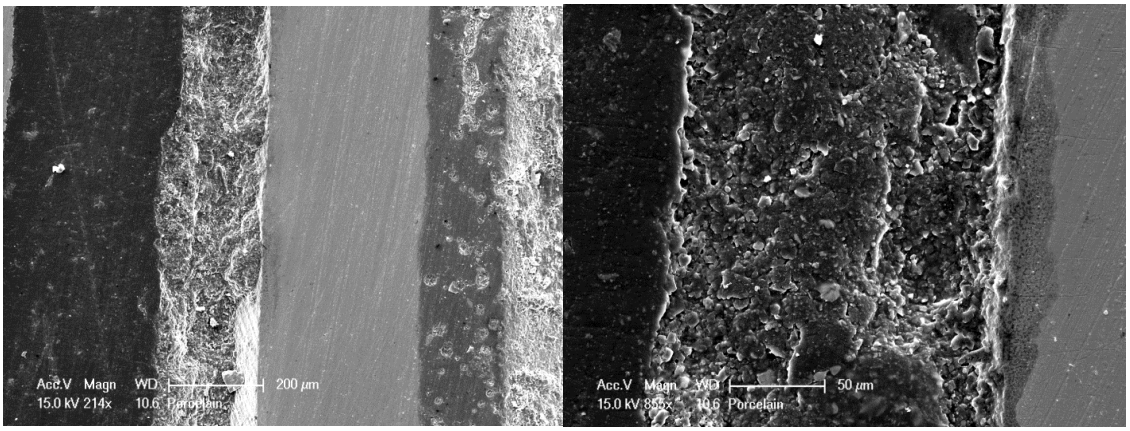

Fig 17 SEM image of the mild steel coated by Porcelain and dipped into the $NaNo_3$(98%)-NaOH(2%) molten salt. The solidified salt layer can be seen in two different magnifications.

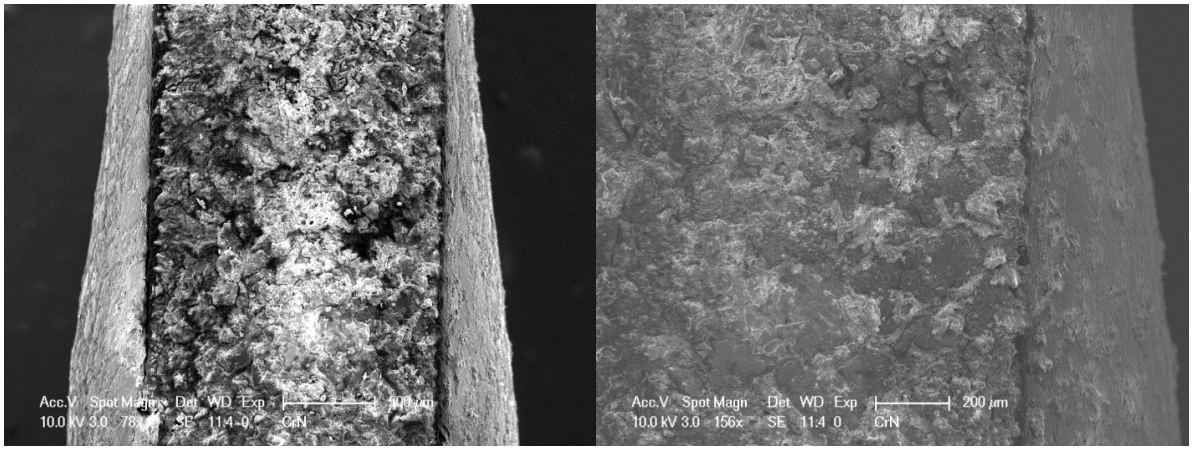

Fig 18 SEM image of the mild steel coated by CrN and dipped into the $NaNo_3$(98%)-NaOH(2%) molten salt. The solidified salt layer can be seen in two different magnifications.

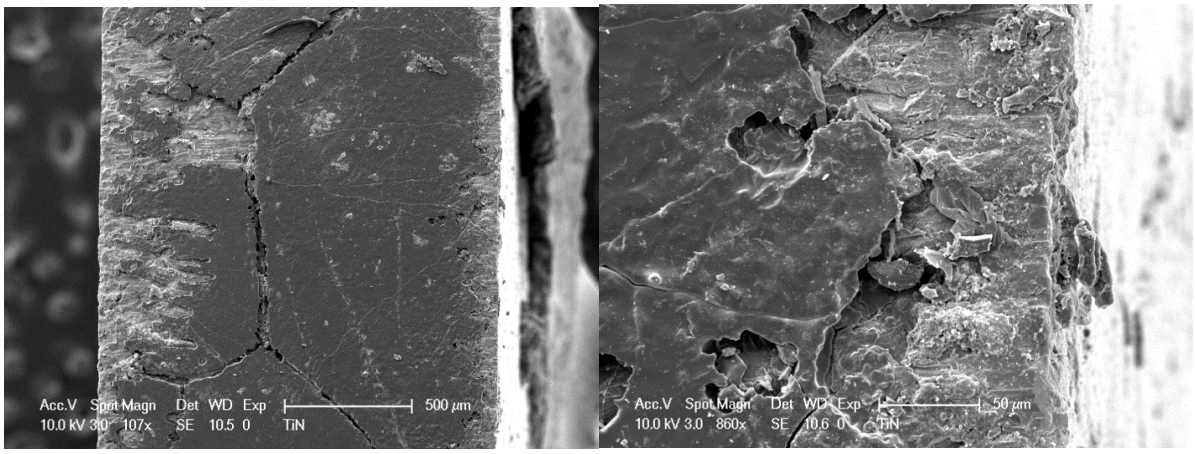

Fig 19 SEM image of the mild steel coated by TiN and dipped into the $NaNo_3$(98%)-NaOH(2%) molten salt. The solidified salt layer can be seen in two different magnifications.

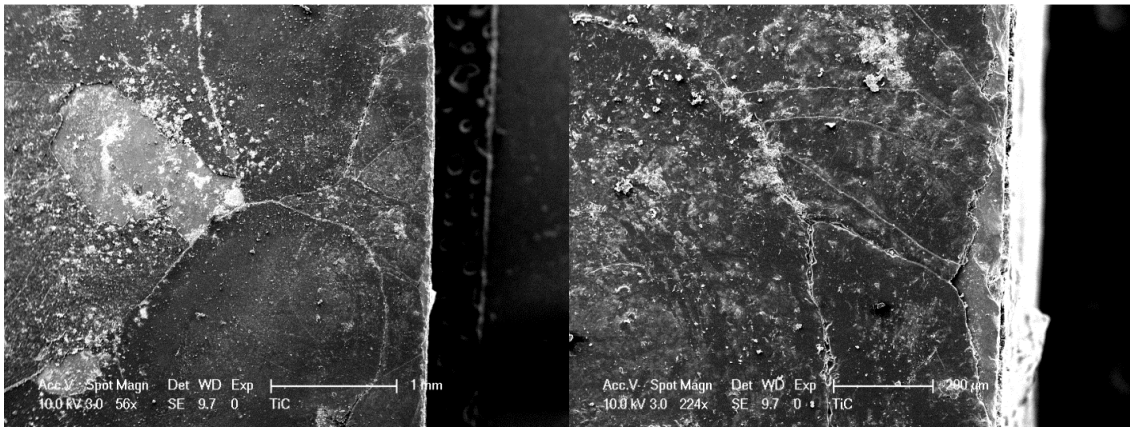

Fig 20 SEM image of the Graphite coated by TiC and dipped into the $NaNo_3$(98%)-NaOH(2%) molten salt. The solidified salt layer can be seen in two different magnifications.

Table 1 Comparing different samples salt layers

Coatings	Mild St/non	Mild St/Porcelain	Mild St/CrN	Mild St/TiN	Graphite/TiC
Sample thickness	1.25 mm	0.7 mm	1.5 mm	1.5 mm	10 mm
Salt layer thickness	187 µm	200 µm	333 µm	125 µm	57 µm

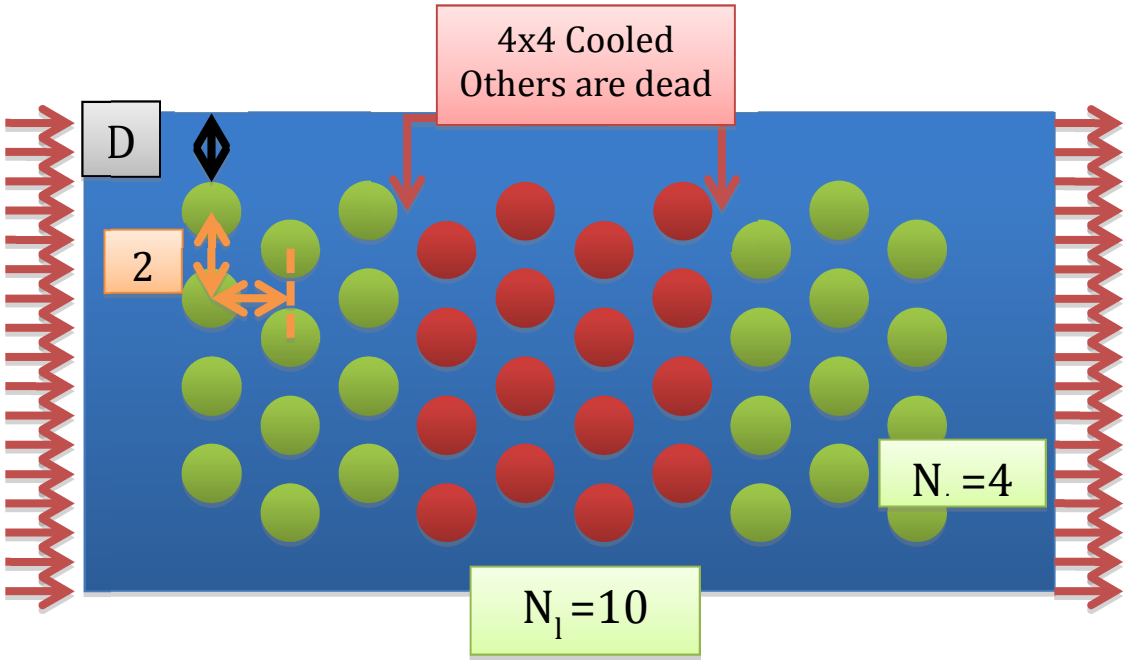

Table 1 above, shows the measured thickness of salt layer on each of the surfaces. According to the results on table 1, TiC coating has the lowest salt layer thickness while the mild steel surface has the highest. The lower thickness of salt may indicate either the salt removal when material was stirred or could be due to the amount salt held by surface tension forces when the sample was retrieved or could be due to cooling and exposure time. The TiC coating may be a promising candidate based on the visual observation of the surface and surface finish and the lower thickness of the coating which may indicate salt removed during stirring.

In addition to salt layer thickness, solidification morphology on different samples was studied. Fig 21 shows the main observed ones.

The bottom right coating with dendrite salt crystals may be better for removal with fluid flow force. However, if this grows uncontrolled and we are unable to break the structure in the early stages of formation, then it can form a strong mesh structure. The space between the dendrite may have been the equilibrium liquid which froze when the sample were cooled down. We will continue to study these morphologies using controlled and re-producible experiments.

Candidate Coatings for Tests with 'Flow-Rig' Heat Exchanger

Based on tests and our interpretation of the results from these tests, we selected the following three coatings for further evaluation with the 'flow-rig' experiment.

- Titanium Carbide Coating on Stainless Steel
- Titanium Nitride on Stainless Steel
- Chromium Nitride on Stainless Steel

Stainless is recommended for the flow-rig experiment to prevent or reduce corrosion. The entire flow-rig is constructed using stainless steel. We will continue to investigate by dip tests the following coatings:

- Cubic Boron Nitride Coatings on graphite or stainless steel
- Cerablack TM coating (proprietary to vendor)
- SGI 400 HR another vendor proprietary hydrophobic coating used on heat exchangers

If any of these show promise we will evaluate them using the flow-rig. The flow-rig is designed to replace tubes easily to conduct qualitative coating tests and measure temperature rise in the fluid inside the coated tube. The temperature rise will provide a relative quantitative measure on *stickability* of salt.

For the final selected coating, we will determine the best thickness of coating, method for depositing the coating and the substrate finish required to meet the performance objective. This will be done prior to building the Phase III engineering model design.

A Note on Candidate Coatings for the Dilute Eutectic Mixture:

It was deemed necessary to investigate further and with more detailed experimentation than the initial results provided by JPL with the dip tests. The effort included electropolishing the samples, setting up the vacuum chamber, making the coatings (evaporation and/or sputtering), testing them with DSC, and analyzing the surfaces and samples by optical microscopy, SEM, and profilometry.

The coating experiments were conducted with pure NaNO3. Even though these coatings performed well with sodium nitrate, adding a small amount of sodium hydroxide caused pitting and the coatings did not survive the attack.

Additional tests were carried out using differential scanning calorimeter to screen coatings for use the dilute eutectic mixture. As discussed in Section 3, chromium coatings were selected as preferred coating.

Seamless stainless steel tubes were first electropolished and chromium is deposited on the tubes. The method and amount of chromium made a difference as discussed in Section 3.

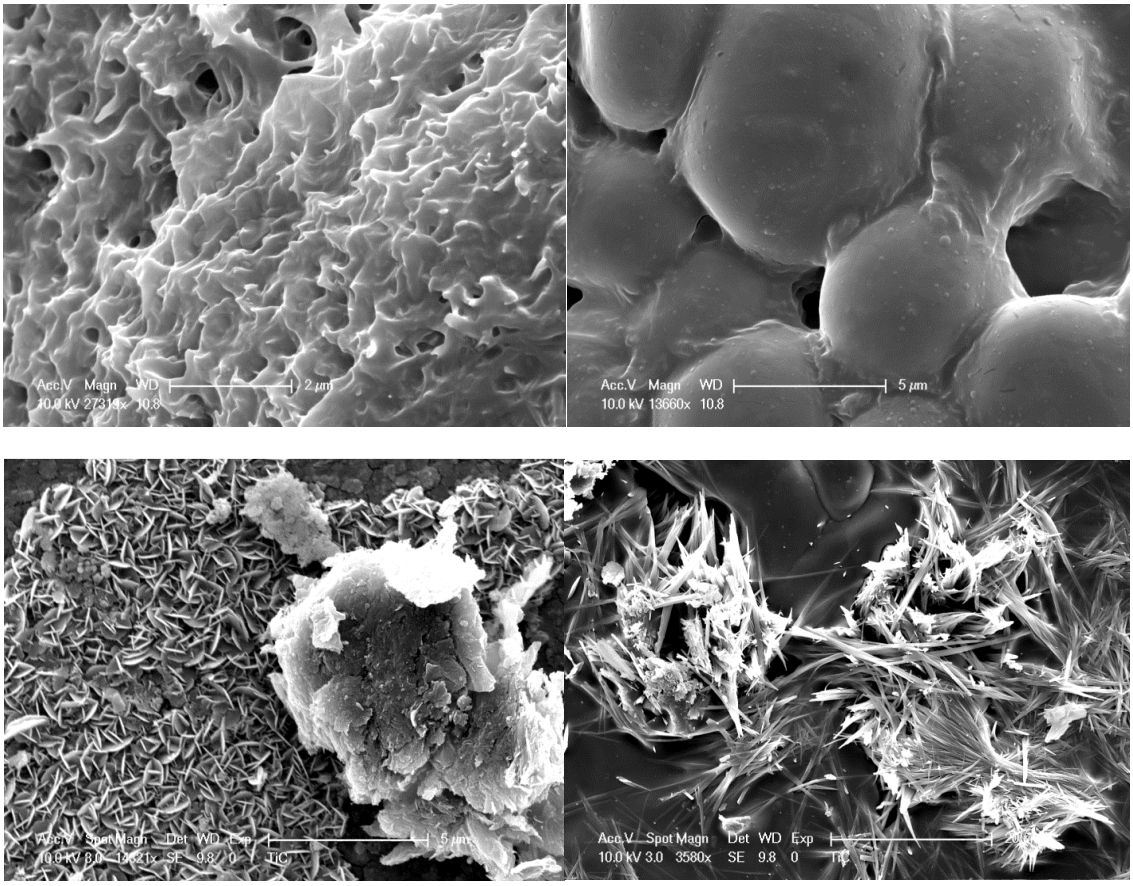

Figure 21. Main salt solidification morphologies observed by SEM

Surface Physical Chemistry – Properties of Coatings Likely to Influence Stickiness of Crystallizing Molten Salt on Heat Exchanger Tubes

Andrew Kindler, JPL

When a crystallizing molten salt is in contact with a heat exchanger tube, there are gradual accumulations of crystals that stick to the outer portion of the tube and impede heat transfer. In order to prevent accumulation of these crystals, both the surface (physical) chemistry and the surface morphology of the tube and crystals must be taken into account. Below the influence of two surface properties on adhesion of crystallites is summarized and related to the choice of material screening test for the heat exchanger.

There are two properties that are likely to influence crystal adhesion: 1) Surface energy of the crystal and heat exchanger surface, and 2) Presence of defects on the heat exchanger surface that are likely to precipitate nucleation there. A simple contact angle test may be insufficient to determine a suitable heat exchanger material.

Surface Energy

The surface energy is the property that determines the surface tension. High surface energy materials like clean metal surfaces have high surface tension. Practically, this means that the interatomic forces of attraction within the metal are relatively high. It also means that the attractive forces relative to anything in contact with it will also be high. Based on this characteristic alone, one might prefer a low energy surface to discourage adhesion. A good example of such a surface is Teflon. Although it is not useful at our operating temperature, it is a low energy surface, and is known for its non stick properties. Such surfaces can be characterized by the contact angle of a liquid on the surface to be tested. A high contact angle (beading up) of a liquid drop on the solid surface is generally indicative of low surface energy of the solid. To be more precise, the surface tension of the solid is low relative to the liquid. If both liquid and solid have the same surface tension, there will be no beading. In our system, we might look for a solid that has low surface tension relative to the molten salt and characterize it by the contact angle of the molten salt on the surface of the solid. This characterization may not be sufficient.

It is not, after all, the molten salt that is sticking to the heat exchanger it is the crystal. The crystal is irregularly shaped, so it is unlikely to have excellent contact with the heat exchanger surface. Even if the crystal has the same surface energy as the liquid (uncertain) its effective surface tension is lower because only a small part of the crystal may have intimate contact with the surface. In other words, the stickiness of the crystals relative to the heat exchanger may be not play as great a role as one imagines. If such is the case, an interesting outcome is possible. You might actually find that a high surface energy surface (as well as a low one) discourages the adhesion of crystals! The reason for this is that the liquid will make more intimate contact with the heat exchanger surface. The intermolecular forces binding the liquid to that surface are greater than that binding the crystal. This means that the crystals will be displaced by the liquid. In this scenario, the greater the attractive intermolecular forces emanating from the heat exchanger made of high surface energy material, the more likely it is to physically bond with the liquid rather at the expense of the solid. From this discussion, you could conclude that both very low energy surfaces and very high energy surfaces could prevent adhesion of crystals. In such a case, you would look for both beading of the molten salt on the surface, or complete wetting. In view of this

conclusion, a contact angle test might not be sufficiently definitive to select a material. Additionally, there is another issue discussed below.

Morphology

Surfaces can be smooth, rough, or even porous. The morphology of the surface is very important. The reason is, rough or porous surfaces offer nucleation sites for the growth of crystals. If a crystal is nucleated on the surface, it is likely to stick. Nucleation sites can be regarded a "sticky" because they allow the forming crystal to drop to a lower energy state than in other locations. If this is the dominant mode of accretion, preparing the surface so that it is extremely smooth is advantageous. Additionally, a low energy surface would be the best choice because the nucleation sites remaining would be far less effective.

Observations

Although both low and high energy surfaces may prevent crystals in the molten salt from depositing on the heat exchanger, preventing nucleation is best accomplished with a very smooth low energy surface. Because it is not known, whether nucleation at the surface is a dominant mode, it is not entirely clear whether we want a low or high energy surface. A contact angle measurement to screen for low energy surfaces may overlook useful high energy surfaces that do not accumulate crystals. A more reliable test for heat exchanger coatings is to immerse a coupon in the crystallizing molten salt and actually test how effective a coating it is. Another possible approach is to correlate the immersion test with the contact angle test for both high and low surface energy surfaces to see which one works best. After this determination, contact angle can be used as a more rapid screening method.

Electrochemical Polishing Parameters for Stainless Steel Tubes

Dr. H. Venkatasetty

316 Stainless tube materials are attractive for heat transfer in high temperature thermal energy storage systems. However, most metals and alloys (including stainless steels), have many surface impurities and/or defects such as metal oxides, foreign particles and stress points which result in poor thermal conductivity and are to prone to corrosion. Electrochemical polishing of surfaces is a well established technique used in industry to produce bright and shiny surfaces suitable for commercial applications. In the case of stainless steel, electrochemical polishing has the potential to provide passive surface with improved corrosion resistance and enhanced thermal conductivity.

With a view to develop suitable electrolyte solutions and experimental parameters for obtaining optimum surface characteristics for 316 stainless steel, we prepared several electrolyte solutions using pure Sulfuric acid and Phosphoric acid and their mixtures with de-ionized water as shown in Table 1.

Table 1. Electrolyte solutions with de-ionized water and Electropolishing parameters

Electrolyte Solution	Composition	Electropolishing time
1.Sulfuric acid	68% by volume	10 & 20 mins
2.Sulfuric acid	40% by volume	3, 5, 10 and 15 mins
3.Phosphoric acid	5% volume	10 and 20 mins
4.Phosphoric acid	50% by volume	10 and 20 mins
5.Phosphoric and Sulfuric acid	60% and 20% vol	25 and 30 mins
6.Phosphoric and Sulfuric acid	40% and 40% vol	8, 10, 20, 25 and 30 mins

316 stainless steel substrates were obtained and their surfaces were cleaned with distilled water and isopropyl alcohol and dried. Digital images of the surfaces were obtained. The cleaned substrate was made the working electrode (anode), the counter electrode (cathode) was a larger size stainless steel substrate and the reference electrode was a Saturated Calomel Electrode (SCE). The electrodes were placed in a suitable container with the electrolyte solution. Using the laboratory Electrochemical Instrumentation, the voltage on the working electrode was slowly increased while monitoring the cell current till the current showed a rapid increase and the voltage was set at a known value and the electrochemical polishing continued for known periods of time. The experiments were conducted at different voltages namely 1.4 V, 1.53 V, 1.6 V and 2.1 V at room temperature. The experiment was stopped at known time interval and the samples were cleaned and dried and the surfaces were examined in the microscope and the digital images were taken. The compositions of the electrolyte solutions and electrochemical polishing parameters are shown in Table 1. Digital images of 316 stainless steel, initial and electrochemically polished for different times in Sulfuric, Phosphoric acid and their mixtures are shown in Figures 22 to 31.

The results of these experiments show considerable improvements of the surface characteristics of substrates after electropolishing in many of the electrolyte solutions particularly from 8 to 30 minutes in sulfuric acid solutions at 40, 50 and 68% by volume. Similarly, Phosphoric acid at 50 % by volume and Phosphoric acid and Sulfuric acid and the mixtures 60 % and 20 % by Volume respectively for 10 and 20 minutes shows promising results. However, it was found that the electrolyte solution with 40% volume

Phosphoric acid and 40% volume Sulfuric acid on electropolishing at 2.1 V for 8 minutes shows much better surface characteristics such as shiny and smooth surface (Figures 9,10).

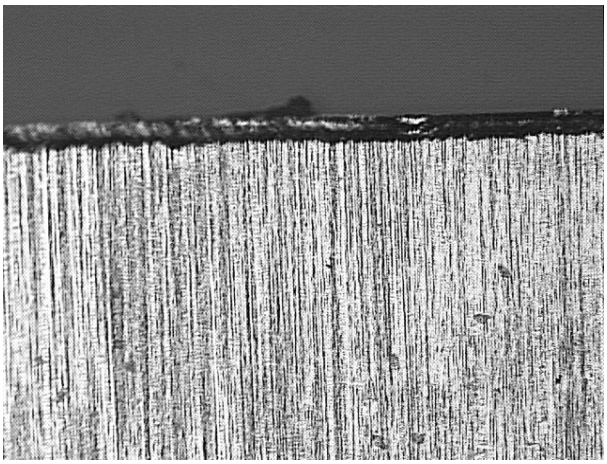

Figure 22. Initial surface characteristics of the Sample . 100X

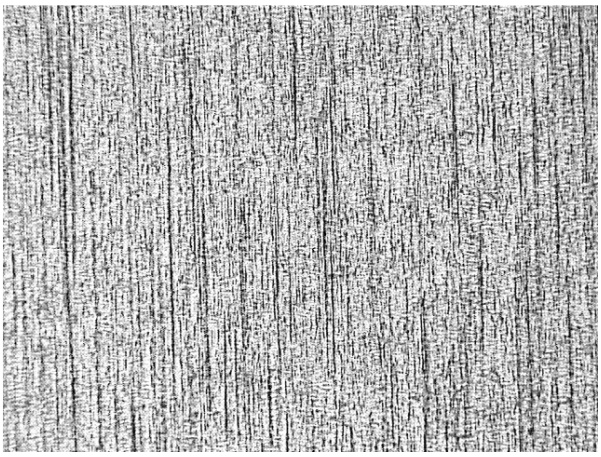

Figure 23. Electropolishing in 40% Sulfuric acid for 5 minutes, center of Sample. 100X

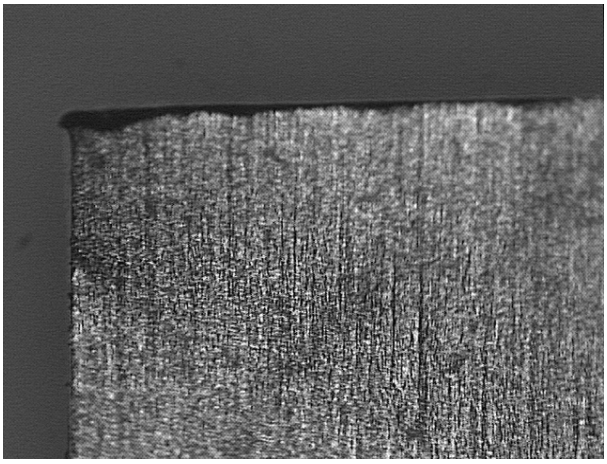

Figure 24. Electropolishing in 40% Sulfuric acid for 10 minutes. 100X

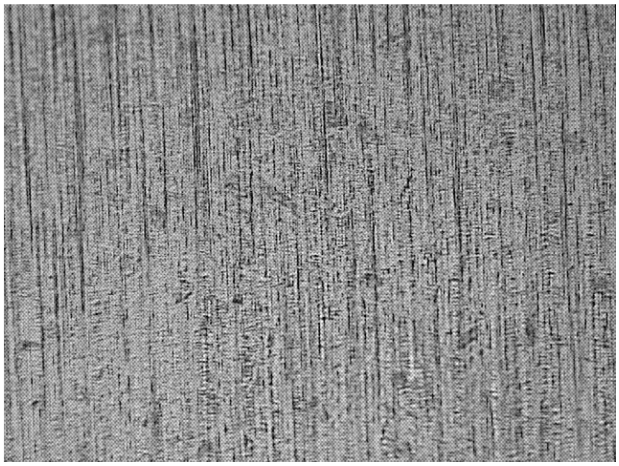

Figure 25. Electropolishing in 68% Sulfuric acid, for 10 minutes. 100X

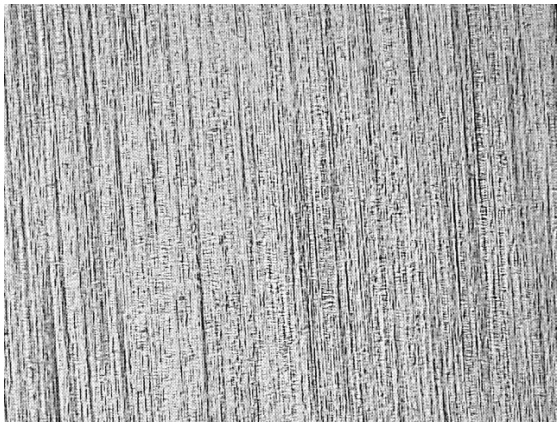

Figure 26. Electropolishing in 5 % Phosphoric acid for 20 minutes. 100X

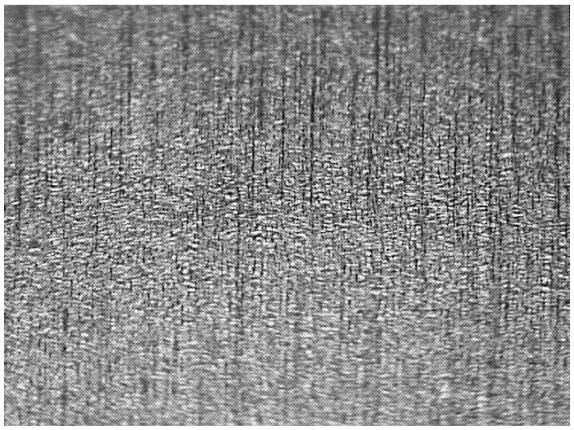

Figure 27 Electropolishing in 50% Phosphoric acid for 20 minutes. 100X

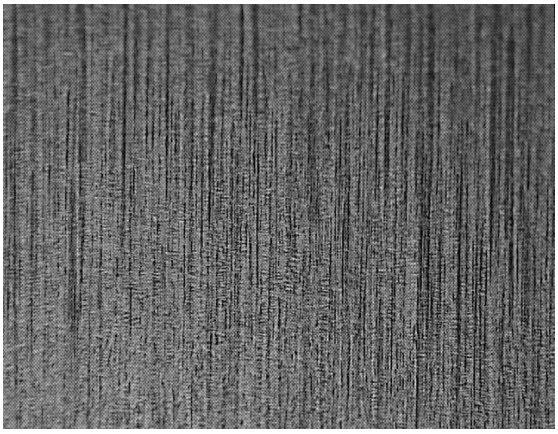

Figure 28. Electropolishing in 60% Phosphoric acid and 20% Sulfuric acid for 15 min. 100X

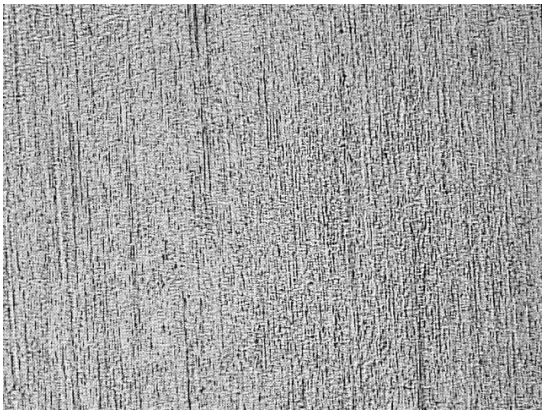

Figure 29. Electropolishing in 60% Sulfuric acid and 20% Phoshoric acid for 30 minutes. 100X

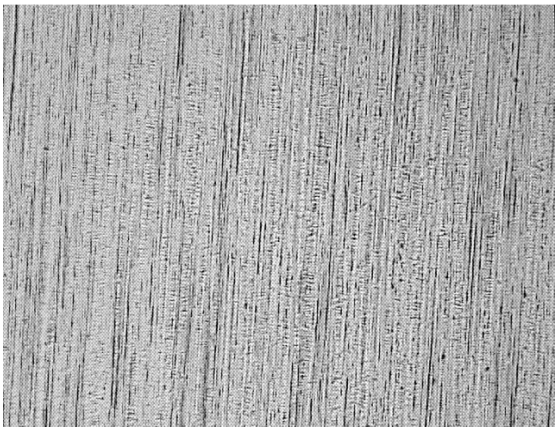

Figure 30. Electropolishing at 2.1 V in Phosphoric/Sulfuric acid 40/40/20 for 8 minutes. 100X

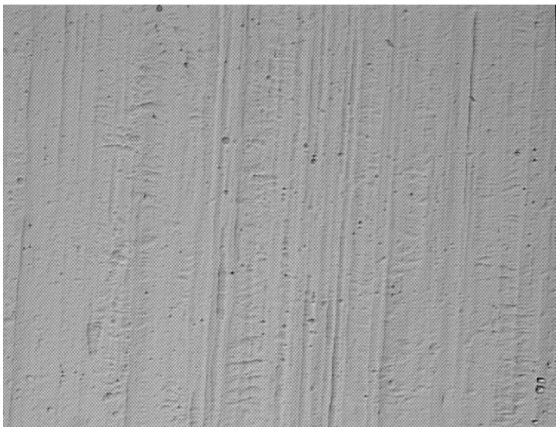

Figure 31. Electropolishing at 2.1 V in Phosphoric/Sulfuric acid 40/40/20 for 8 minutes. 500X

Appendix 3
Design of Laboratory Scale Prototype

By Corey Hardin

This section focuses on the design of the experiment apparatus for studying the heat transfer performance in latent heat storage systems. The report begins with a baseline analysis balancing predicted overall heat transfer coefficient and solidification with heat exchanger area. After this, more detailed analysis is presented to analyze the effects of tube size on Reynolds number, pressure drop, % *solidification, etc. The purpose of this is to establish a baseline of calculations for further detailed design to follow. The analysis assumes cross flow, which should be analogous to a baffled shell and tube heat exchanger.*

Introductory Analysis

To begin our analysis we will present a baseline energy balance calculation. We balance the overall heat transfer rate with the energy it takes to bring the salt down to melting temperature and achieve a solid fraction of 20%. For the purposes of this calculation we assume tubes of 0.375" OD, and a channel cross section of 10 diameters square (i.e., 3.75" x 3.75"). We account for 50% of this area being blocked by tubes giving us a cross sectional area, A_c, of .009 m^2*50%. We also assume an overall ΔT of 15 degrees Celsius between salt and tube walls, and an inlet superheat of 5 degrees Celsius.

$$\dot{Q} = hA_s\Delta T = \dot{m}\left(C_pT_{superheat} + H_f\varphi\right) = \left(\rho A_c V\right)\left(C_pT_{superheat} + H_f\varphi\right)$$

h (W/m^2K)	500
ΔT (C)	15
C_p (kJ/kgK)	1.821
$T_{superheat}$ (C)	5
H_f (kJ/kg)	174
ϕ (% Solid)	20%
ρ (kg/m^3)	2260
A_c (m^2)	.009*50%

From this we are left two independent variables: heat exchanger surface area A_s and salt velocity V. If we assume a velocity of 1 m/s (Re_D=8300), Q works out to 450 kW, which leads us to a heat exchanger area of 60 m^2. This means for an array of 40 cooled tubes we would need over 525 passes to achieve the desired solid fraction. Alternatively, we could achieve the desired 20% solid fraction at only 14 kW if we decreased the salt velocity to 0.03 m/s; however in this case the salt-side Reynolds number would be only 250.

Importance of Reynolds Number

The capability of operating at high Reynolds number is an important functionality for this apparatus for two major reasons:

(i) To ensure that we can produce the hydrodynamic forces that will be necessary to achieve "flaking" of the salt off of the tube. The larger the range of Reynolds numbers we can test, the larger the range of coatings we will be able to test. Even if our coatings fail to flake at industrially viable Reynolds numbers, if we can prove that flaking will occur at higher Reynolds numbers this will be proof that our concept is viable. From a scientific perspective if we could hit a high enough Reynolds number to flake off of a plain or coated steel tube, we could begin to perform a thorough study in which we could possibly come up a with a formula to relate coating surface energy to Reynolds number necessary for flaking. This would make heat exchanger design for the full scale system very simple. On the other end, if we don't give ourselves the capability of high Reynolds numbers we may fail to create the flaking phenomenon at all.

(ii) Scaling to match full-size heat exchangers. Basic on initial familiarity with typical full-scale heat exchangers involving molten salt, we expect that a typical Reynolds number is in the range of 20,000. Also, typical convection design curves for staggered tube banks and shell & tube heat exchangers show a transition in behavior at around $Re_D \approx 1{,}000$, in terms of both pressure drop and heat transfer [ref. *Perry's ChemE Handbook*; Zukauskas in Hartnett & Irvine *Adv. Heat Transf*]. Therefore, to be able to match the approximate operating conditions of a full-scale heat exchanger, it is important for this apparatus to be capable of operating in the ReD range of several 1,000 at the very least, and with a strong preference to reach the range of 20,000+.

Heat Transfer Fluid Selection

We first performed a study to analyze the affects of using various different heat transfer fluids to determine which would be most effective for use in the phase 2 apparatus. The fluids analyzed were air, helium, compressed air, compressed helium, and Therminol 66. Of these, Therminol 66 and compressed helium both showed excellent heat transfer characteristics while having distinct advantages and disadvantages in other areas. Compressed helium was favorable due to its ease of implementation, without any design research necessary to implement. Leaks are also much easier to deal with, and the system overall would be far less complicated than a Therminol system. It does however suffer from a few drawbacks. The first is that it is not a current staple in power generation, although it has been used as a heat transfer fluid elsewhere. The helium compressor necessary was also considerably more expensive than a heat transfer equivalent Therminol pump and we would have to deal with greater pressures. Therminol has a few drawbacks in that it does require a good amount of research to implement properly, there are more safety issues in design, leaks are far less tolerable, and the system must be much more complex in order to operate safely. In the end Therminol won out over helium due to the fact that it gets higher heat transfer at less cost, is widely used in industry, and works at significantly lower pressures.

Scaling Rules

Before more detailed analysis could be performed, standard scaling parameters had to be established to allow for fair comparison between different tube sizes. A preliminary analysis was performed to determine the best tube arrangement to produce. It was observed that higher tube pitches allowed for higher heat transfer rates with much smaller pressure drops and similar flow rates. It was therefore decided to pick a fairly high pitch to diameter ratio of 2 (table values for heat transfer correlations range from 1.25 to 3). In Incropera and Dewitt's *Introduction to Heat and Mass Transfer* it states that heat transfer conditions do not fully develop until the fourth tube in a bank, therefore it was decided to place 3 dead columns of tubes on each side of the cooled section. If more cooling is required, there are correlations that take into account this entrance region, but they are only valid if you have a minimum of

10 columns. It was therefore decided to do analysis on 4x10 banks of tubes with only the center 4x4 tubes being cooled. Figures 1 and 2 show schematics of the sizing parameters utilized. An overall heat transfer coefficient of 500 W/m^2*k was assumed in all cases.

Although it is understood that the standard correlations may not apply to tubes with a heavy salt coating, we expect that many of the test runs will have a relatively thin salt coating -- ideally no salt layer in the best case -- and thus may be fairly well approximated by the standard correlations.

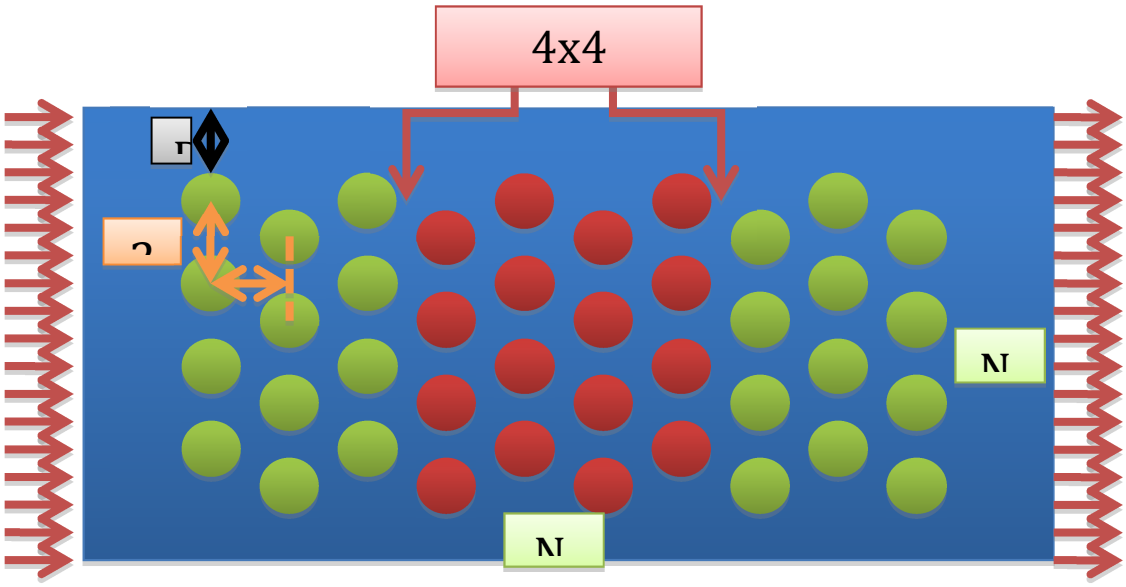

Figure 1: Side View Sizing Schematic

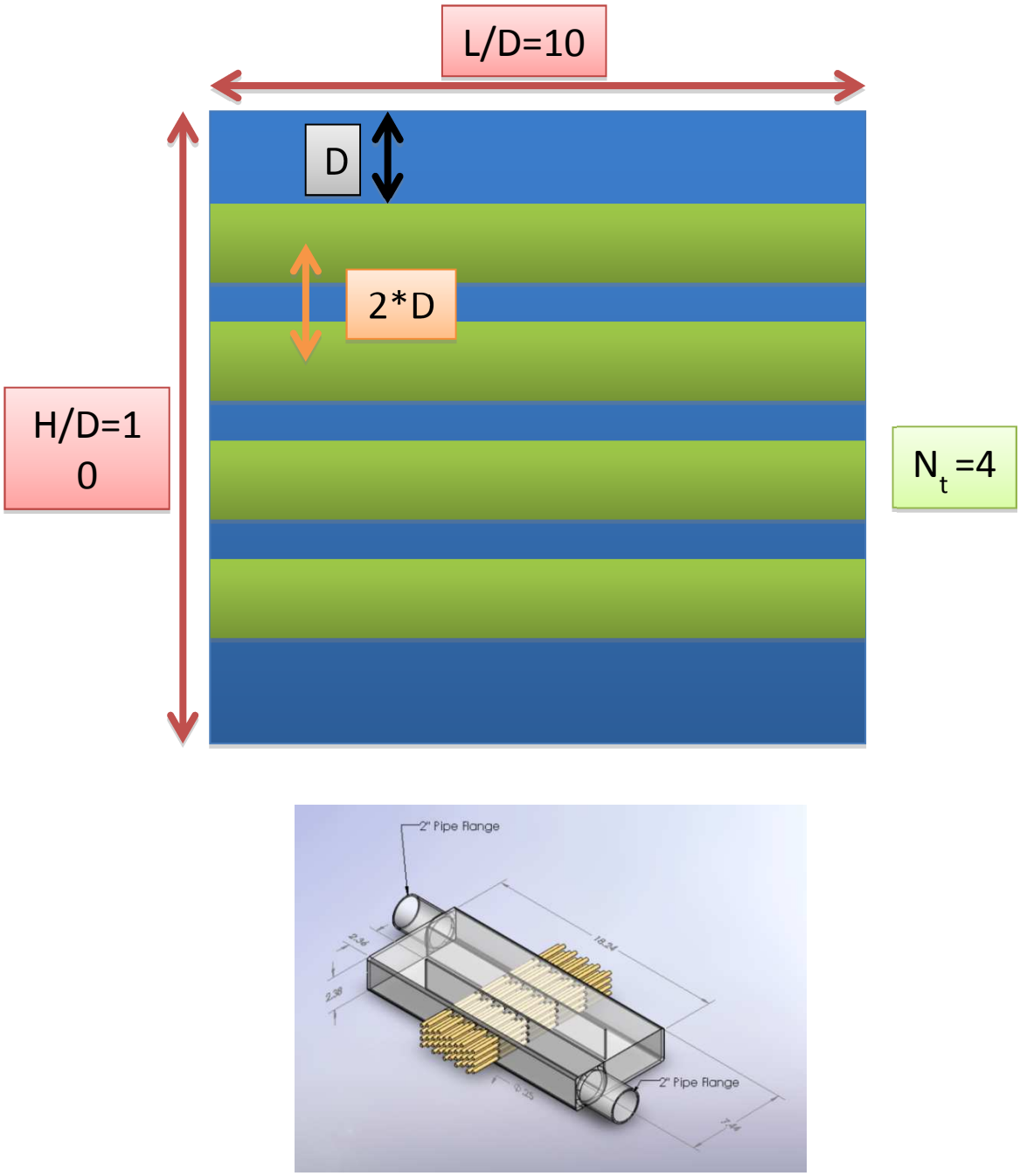

Figure 2: Front View Sizing Schematics and Rendering of Example Heat Exchanger (3 passes shown). In the case of multiple passes, the length allowed for the 180° turns has not been optimized in this schematic.

Salt Flow Analysis

We then went on to analyze the salt flow and heat transfer conditions. A parametric study was performed to study various tube sizes under equivalent dimensionless parameters (Re, Nu, Pr, etc.) The effect of tube size was analyzed versus pressure drop, maximum achievable Reynolds number with current salt pump, change in solid fraction per pass, and overall heat requirement to achieve solid fraction. Plots of all of this analysis can be found in the appendix.

From a pressure drop perspective on the salt side, it was found that a ¼" tube is marginally acceptable with a pressure drop of 12 psi per pass at ReD of 20,000. Larger tube sizes decrease the pressure drop, but increase flow rate requirements. From this perspective it was determined that ½" was the largest tolerable tube size with a maximum ReD of 10,000 with our current pump. If we want Reynolds numbers in the 20,000-30,000 range we will need to get a new pump with either better pressure or flow performance as the ¼" tube barely achieves 20,000 ReD which will most likely be diminished by the large pressure drop.

Solid fractions achievable are fairly small at low delta T and high flow rate. In order to achieve large solid fractions we must do one of 4 strategies.

(i) The first strategy is to use large numbers of passes. This can quickly become impractical however, and in general the number of passes should be kept to a minimum with a maximum of ~5-7.

(ii) The second strategy is to increase delta T. This can be accomplished fairly easily, but produces problems in modeling and solidification conditions.

(iii) The next strategy is to decrease salt flow rate. This decreases the amount of mass that has to be cooled, but also decreases the hydrodynamic forces available to break the salt free from the tube surface, and decreases the salt-side Re_D which is undesirable for reasons of scaling.

(iv) The final strategy would be to rely on increasing the solid fraction a small amount on each pass until the entire system was in slurry form. This would require us to develop a pumpable slurry however that we may not need otherwise.

It must also be taken into account that larger solid fractions require higher heating rates. As tube diameter, and therefore the cross sectional flow area, increases the mass flow rate increases and therefore the more heat it required to achieve the same solid fraction.

Therminol Flow Analysis

On the Therminol side pressure drop was only an issue with 1/8" and smaller diameter tubes. Regarding the flow rate, the smallest pump quoted so far will still perform well in a 4x4 array of 1" tubes. If we decide to cool all 10, we should stay at .5" or smaller in order to maintain a ratio of Therminol convection to overall heat transfer coefficient (h/U) of 10 or greater. Having a high h/U will allow us to better control the wall temperature of the tube, and make it easier to get accurate measurements of the salt side convection coefficient (and solid formation conduction). Temperature rise of the Therminol per pass changes with Reynolds number and tube diameter. The higher the flow rate and the smaller the tube size, the smaller the delta T will be. This creates similar problems to the overall delta T mentioned earlier as well as that the overall delta T will vary as the salt passes over different areas of the tube array which can add error to heat transfer calculations.

Next three different pump curves were obtained from Magnatex Inc. for their three smallest mag-drive high temperature pumps. From the curves the maximum Reynolds number and h/U ratio were calculated. The 1/8" tube produced the highest h/U ratios, but is slightly inefficient in that flow is pressure limited, not flow limited. The ¼" tube and above were flow limited, and with the exception of the 1" tube produced an h/U greater than 10 even for the smallest pump. Below we present more details of the actual design and hardware being installed.

Tank assembly (Solidworks). The brown rectangles are the numerous strip heaters.

Electrical Heaters

One of the lessons from the Phase 1 design was that the heater capacity should be increased significantly, and include immersion heaters as well as external heaters mounted to the outside of the tank and flow sections. This extra heater capacity helps save time when charging and discharging the tank, and allows us to withstand the occasional failure of a few heater elements. Therefore one of the major features of this Phase 2 design is a large amount of heater capacity, exceeding 60 kW, as summarized in the table below.

Type of Heater	Location	Quantity	Capacity (Watts)	Subtotal (Watts
Immersion heaters	Main salt tank	5	1,000	5,000
Strip heaters	Various, mainly tank exterior	42	625	26,250
Strip heaters	Heat exchanger	4	625	2,500
Cartridge heaters	Therminol rig	6	1000	6,000
Tape heaters	Flow sections	4	840	3,360
Band heater	Salt drain	1	2000	2,000
Band heaters	Salt melt tower	8	2300	18,400
Band heaters	Salt melt tower	2	350	700
	TOTALS	72		64,210
		elements		Wattage

Specifying the immersion heaters took considerable time, and we explored various commercial products from companies including Watlow, Tempco, and Hampton Controls. Finally, for reasons of price and availability we elected to have own immersion heaters fabricated based around commercial cartridge heaters using a common specialty machining technique known as gun drilling.

Electrical Infrastructure

Because of the demands of the pump, the desire for large heating capacity described above, and because some of the heaters require 480 V, we had to more than triple the electrical capacity at the experimental working area:

New / Existing	Phase	# of Circuits	Volts	Amps	Watts	
Existing	1	3	240	40	28,800	
Existing	3	1	240	30	7,200	
New	1	4	480	40	76,800	
New	3	1	480	30	14,400	
				TOTAl	127,200	
					Wattage	

This required running new conduit from a CE-CERT transformer to the lab, into a new breaker box and control box, and then on to the experimental station. The previously existing control system was updated to accommodate all of the new heating zones.

Salt Pump

After a time consuming search among possible vendors including Friatech, Lawrence, and Wenesco (lower cost solder pumps), we procured a p ump from Friatech that was specifically designed for molten salts. The pump has salt lubricated bearings and a 20 HP motor. We expect it to provide ~150 GPM at the actual HX head loss. The pump has been installed at CE-CERT and tested with water, and provided over 400 GPM at 60% drive through a test pipe section (not the actual HX).

Friatec Salt Pump. Left: Overview. Right: Detail of flange assembly.

Therminol Pump

The flow loop uses Therminol 66 to on the cold side of the molten salt heat exchanger. The design includes a Therminol reservoir of capacity 55 gallons. The Therminol pump was purchased from Dickow. It is 2 HP with a magnetic drive, and rated to a flowrate of 30 GPM and a maximum temperature of 300 °C. The Therminol pump has been tested successfully.

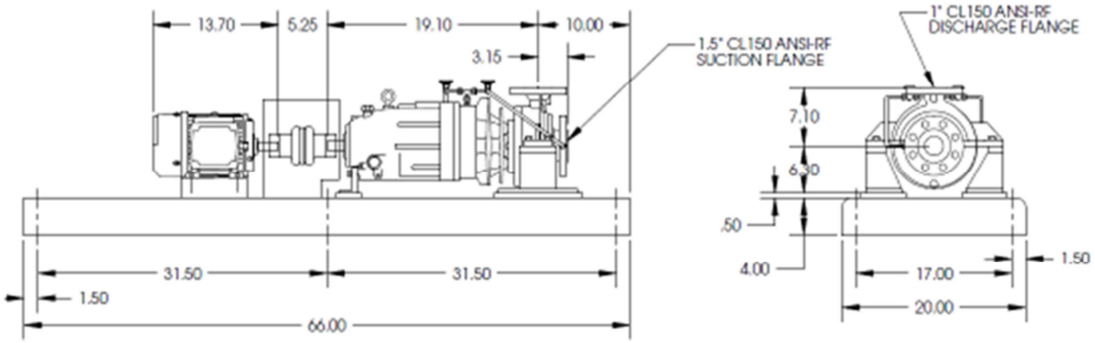

Recommendations and Discussion

From these calculations a tube size of ¼" to ½" is recommended. A ¼" tube size gives a good range of salt Reynolds number, but is limiting on the pressure drop side, and therefore is not recommended for large numbers of passes. A ½" tube size is not nearly as limiting on pressure, but the range of Reynolds number available with our current pump is limited. Therefore from a salt flow perspective, .375" diameter tubes should be optimal. The Therminol flow conditions are adequate over most of the entire size range, so this is not a major factor in the decision.

Table 1: Sizing Calculations Overview

	Tube Diameter	1/8"	¼"	3/8"	1/2"	1"
Salt	Pressure Drop Per Pass (psi)	740	18	8	5	2
	ReDmax at 140 GPM	43000	22000	16000	11000	5500
	ΔSolid Fraction Per Pass @100GPM	0.02	0.04	.06	0.08	0.17
Therminol h/U=10	Pressure Drop Per Pass (psi)	1.2	0.25	.12	0.05	0.01
	GPM	8	20	30	40	80
	ΔT per pass	52	35	34	33	32
Overall	Q (kW)/Pass ΔT=15 (C) ϕ=20%	150	300	450	600	1600
8" Volute 2HP	(Therminol h)/ (Salt-Side U), Max (higher is better)	40	28	22	15	7
10" Volute 2HP		43	33	25	17	9
8" Volute 5HP		49	62	47	31	17

In the end **the heating rate is the largest limiting factor**. Also, there is an important competition between the desire for large change in solid fraction (e.g. input of 5 C superheat and output of 20% solids fraction) and the desire for a high Reynolds number (for reasons of shear stress and scaling similitude). The scientific goals could still largely be studied even in the absence of significant solid fraction. Specifically, for a pure liquid salt and a sub-cooled wall temperature, can we ensure that the solids do NOT nucleate (or build up) on the tube wall? If we do require the high solid fraction, will we rely on pumpable slurry or will we sacrifice Reynolds number? Figure 31 shows how high of a solid fraction we can achieve at Reynolds number for different heating rates for a 0.375" diameter tube. Our system is currently outfitted with approximately 20 kW of heating. We need to decide how much we will need to increase this, taking into account we need heating and cooling on the Therminol loop as well.

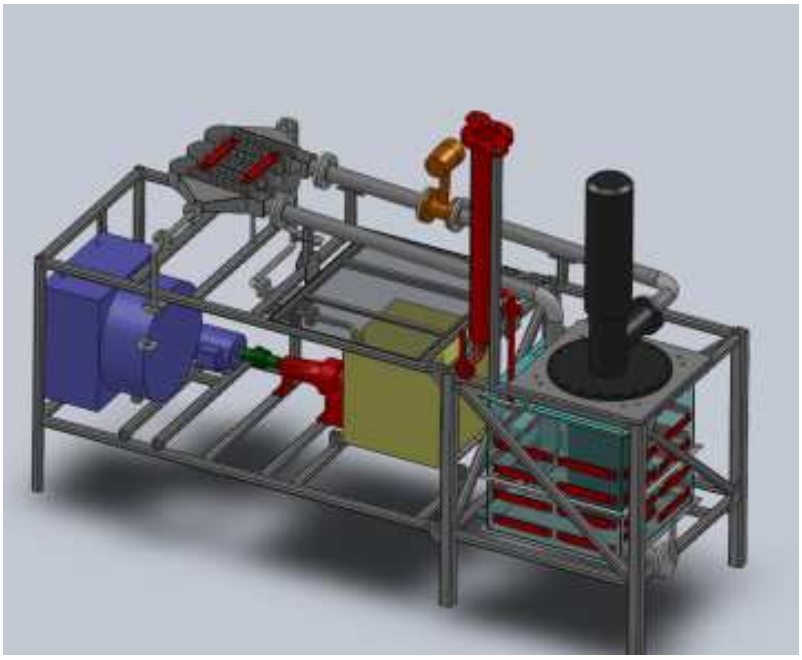

Overview (Solidworks rendering)

Overview (Dec. 2010).

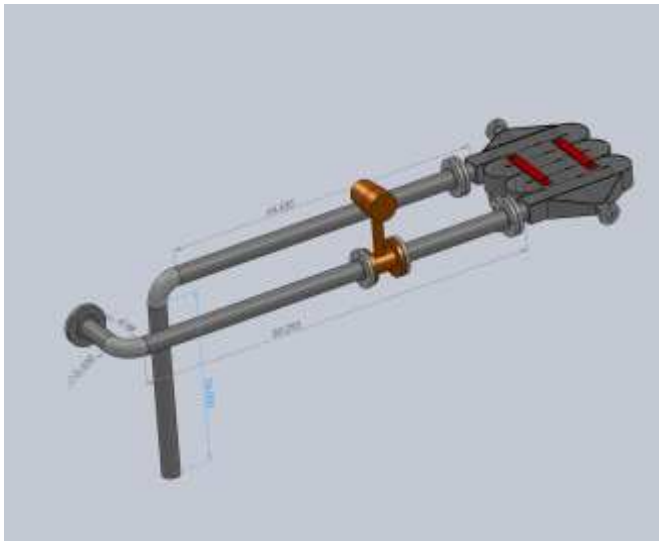

Heat exchanger overview, including inlet and outlet pipe runs and flow meter.

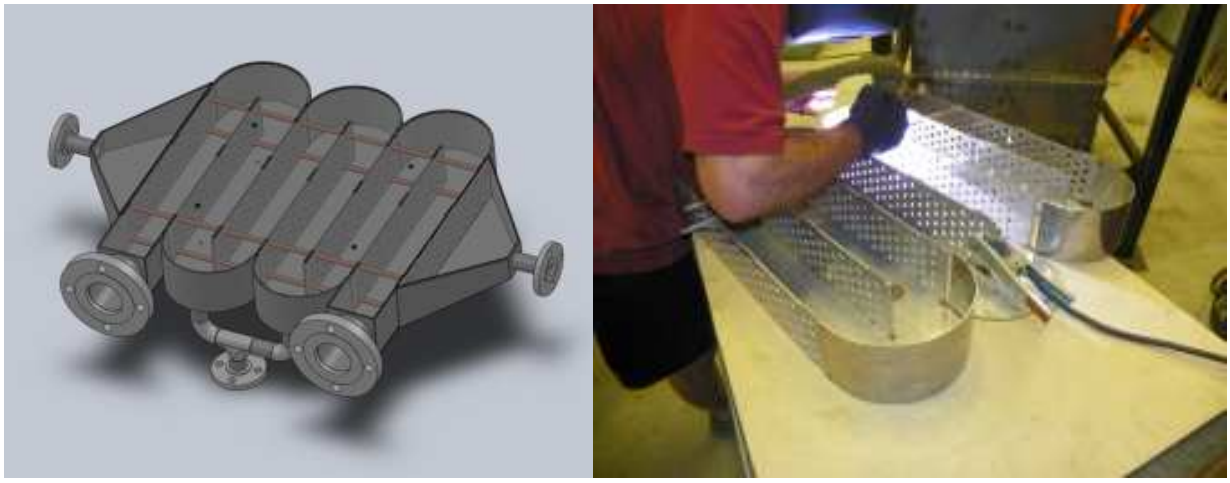

Heat exchanger detail. Left Image: The two large flanges are the inlet and exit for the salt side, which is 6 pass. Only four of the 80 tubes (3/8") are shown (brown cylinders). Right Image: Welding part of the flow section.

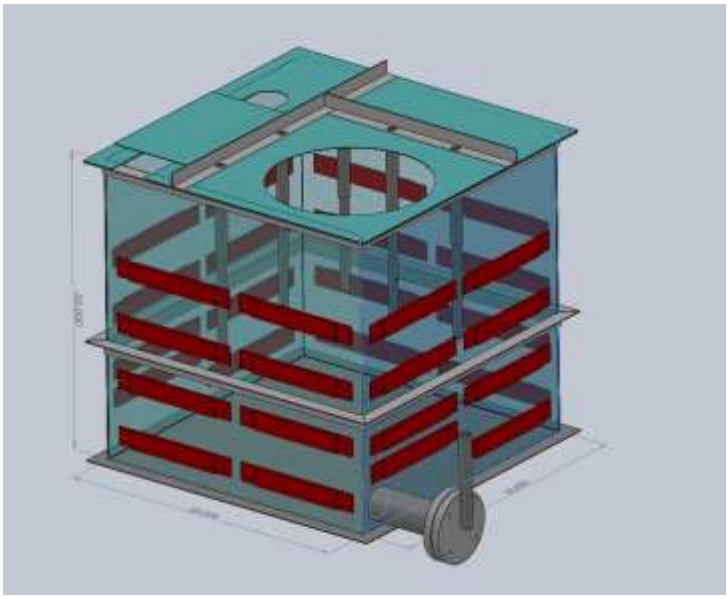

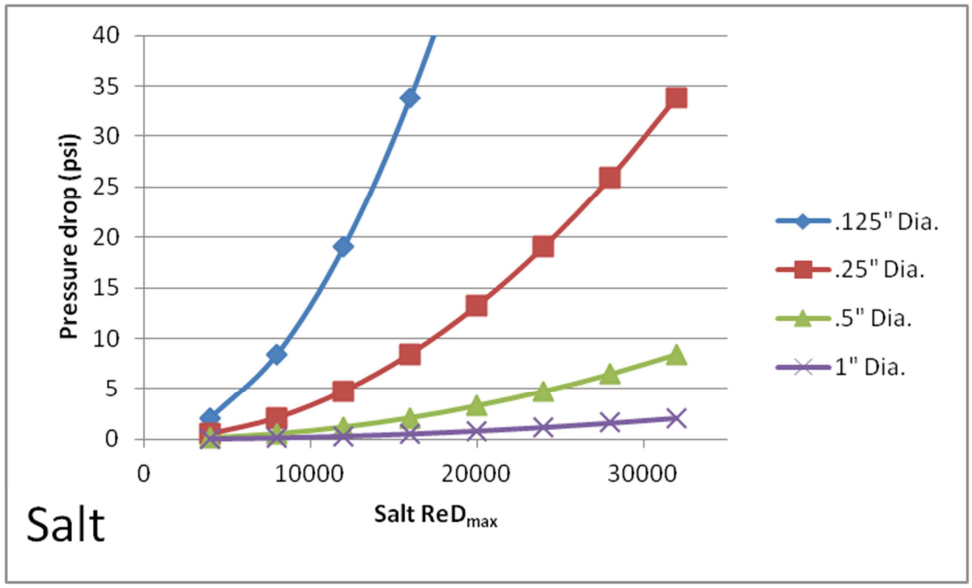

Figure 3: Salt Pressure Drop vs. Reynolds Number

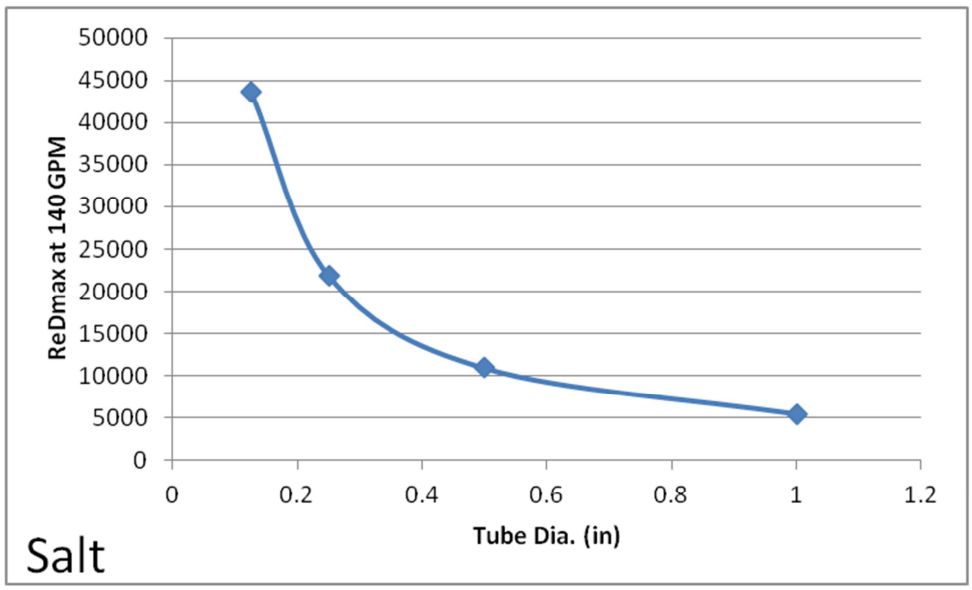

Figure 4: Maximum Salt Side Reynolds Number at Current Pump Maximum Flow Rate vs. Tube Size

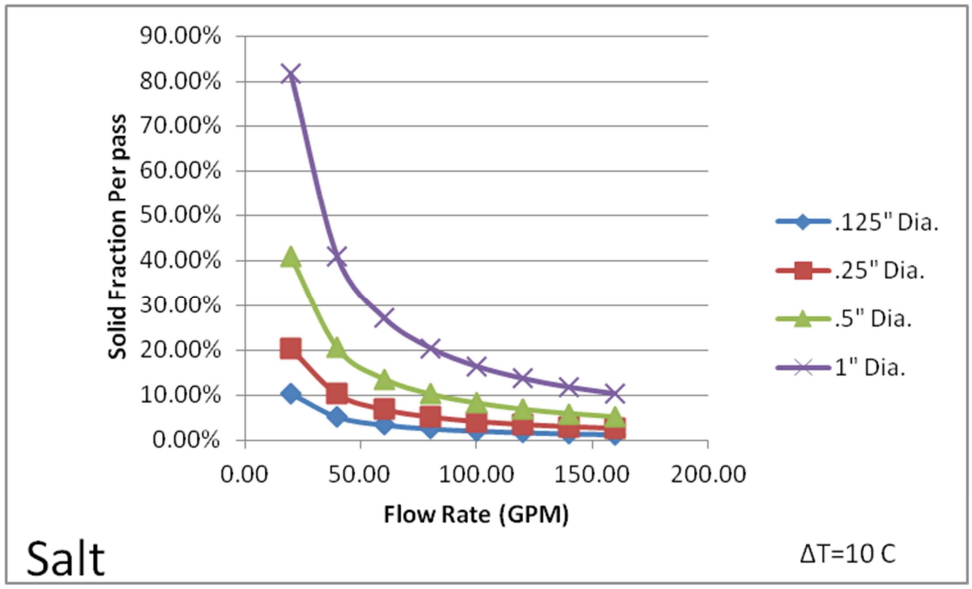

Figure 5: Change in Solid Fraction per Pass vs. Flow Rate and Tube Size

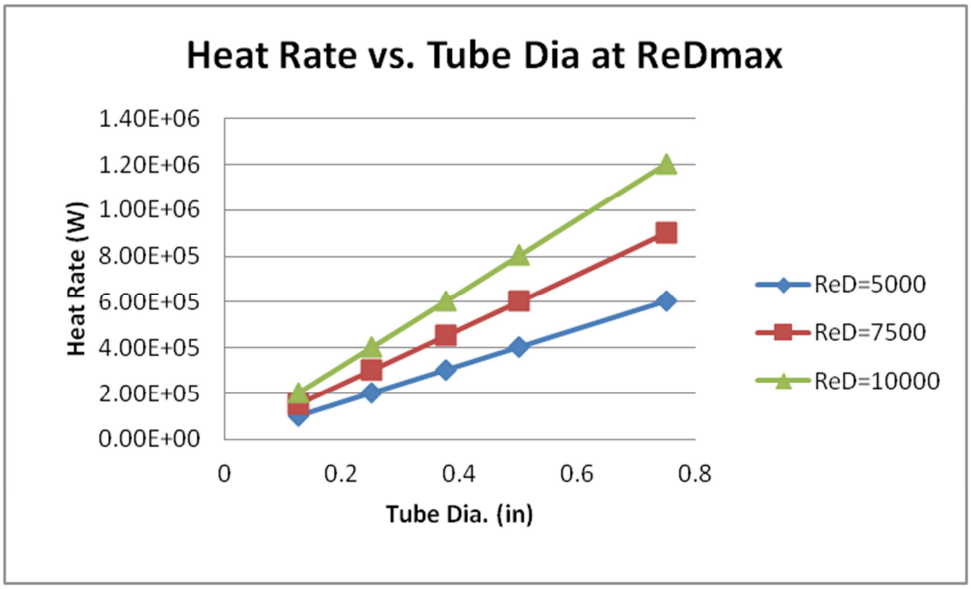

Figure 6: Cooling Rate Required to achieve solid fraction with different tube sizes at different Reynolds numbers

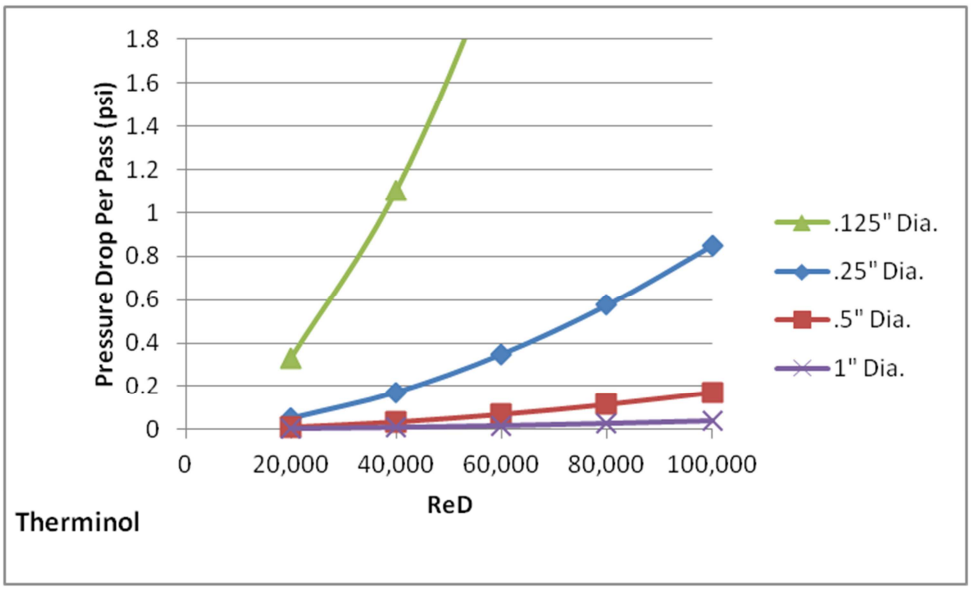

Figure 7: Therminol Pressure Drop Per Pass vs. Reynolds Number and Tube Size

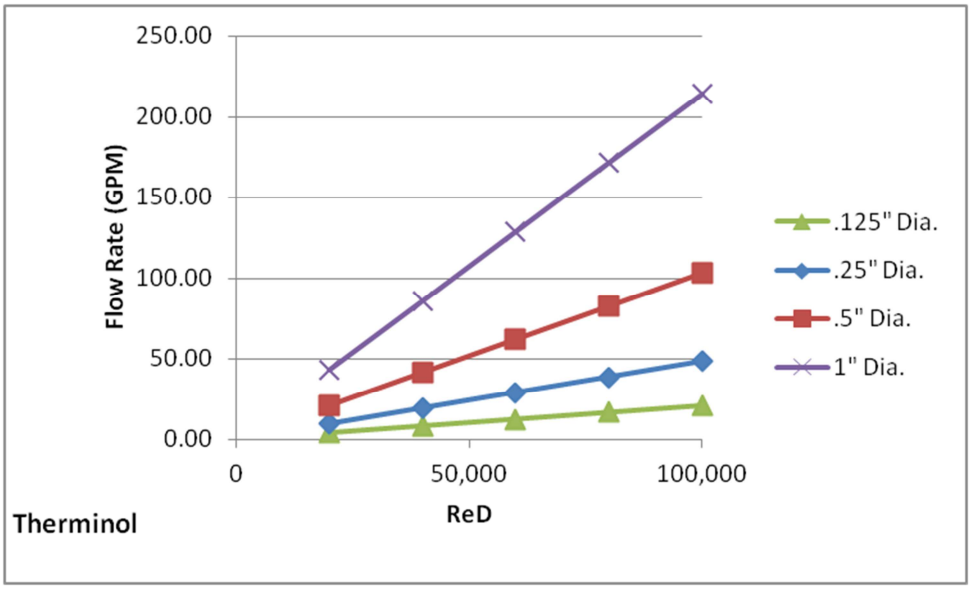

Figure 8: Therminol Flow Rate in GPM vs. Reynolds Number and Tube Size

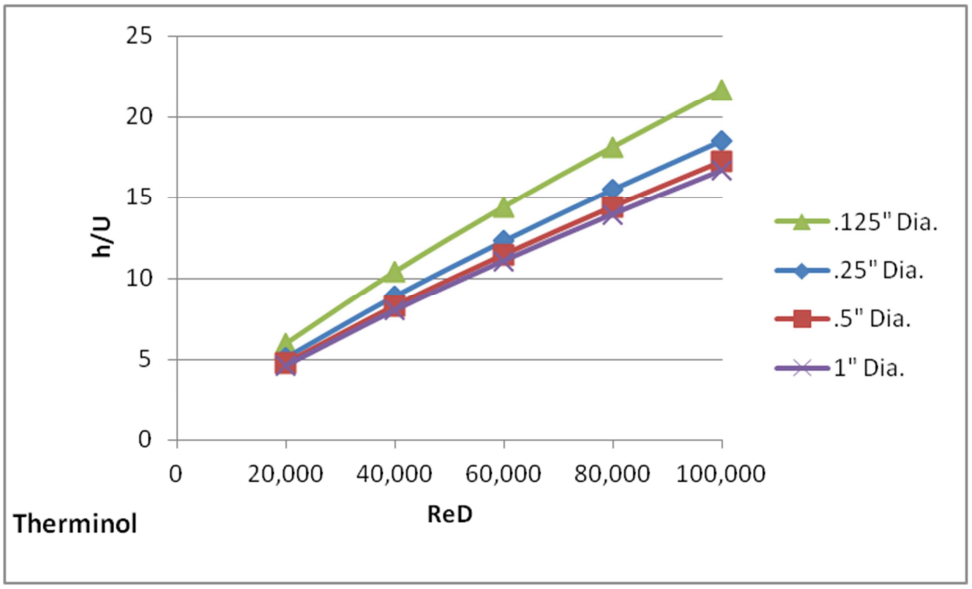

Figure 9: Ratio of Therminol h to Overall U vs. Reynolds Number and Tube Size

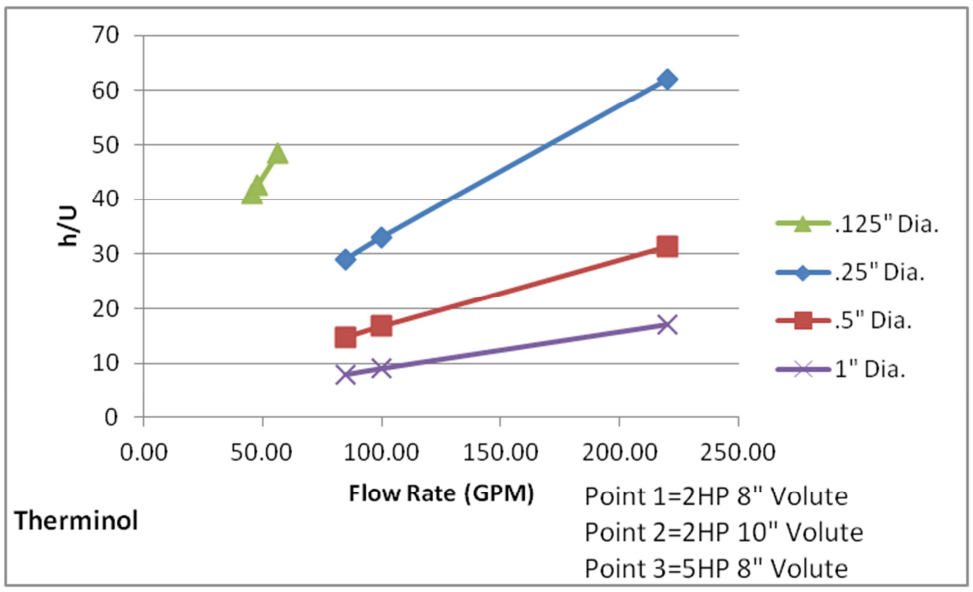

Figure 10: Ratio of Therminol h to Overall U vs. Pump Flow Rate Achievable and Tube Size

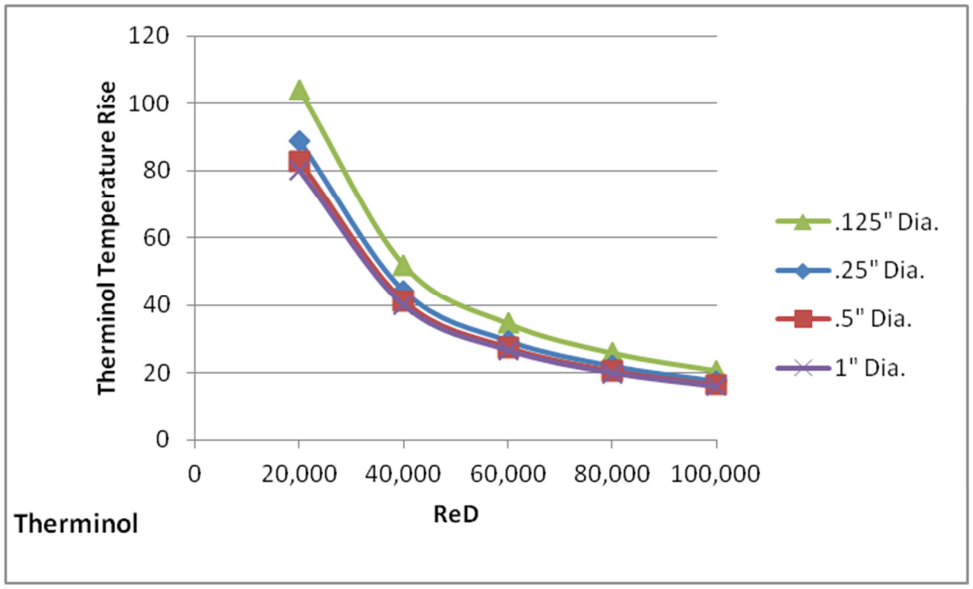

Figure 11: Therminol Temperature Rise per Pass vs. Reynolds Number and Tube Size

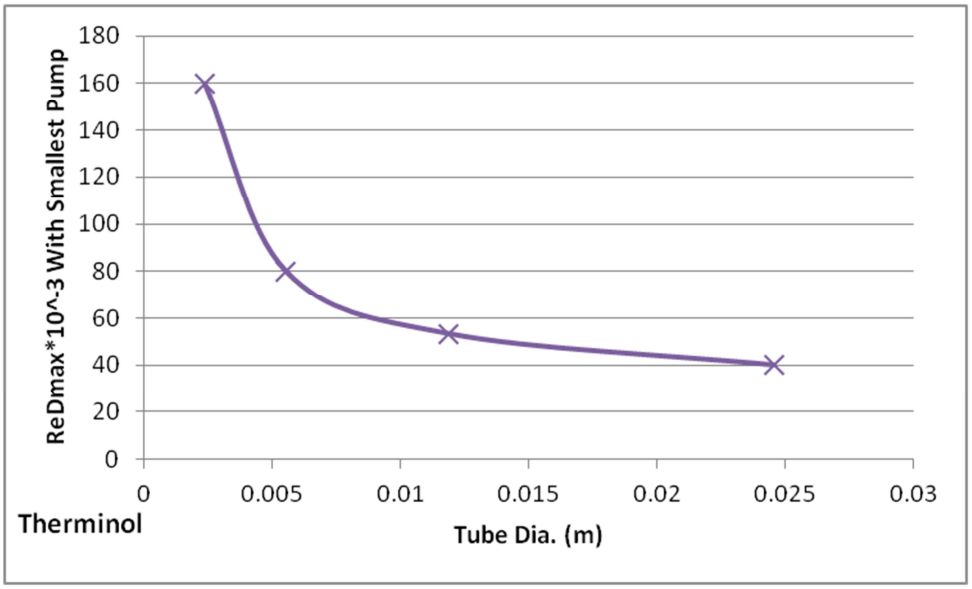

Figure 12: Maximum Reynolds Number Achievable with Smallest Therminol Pump vs. Tube Size

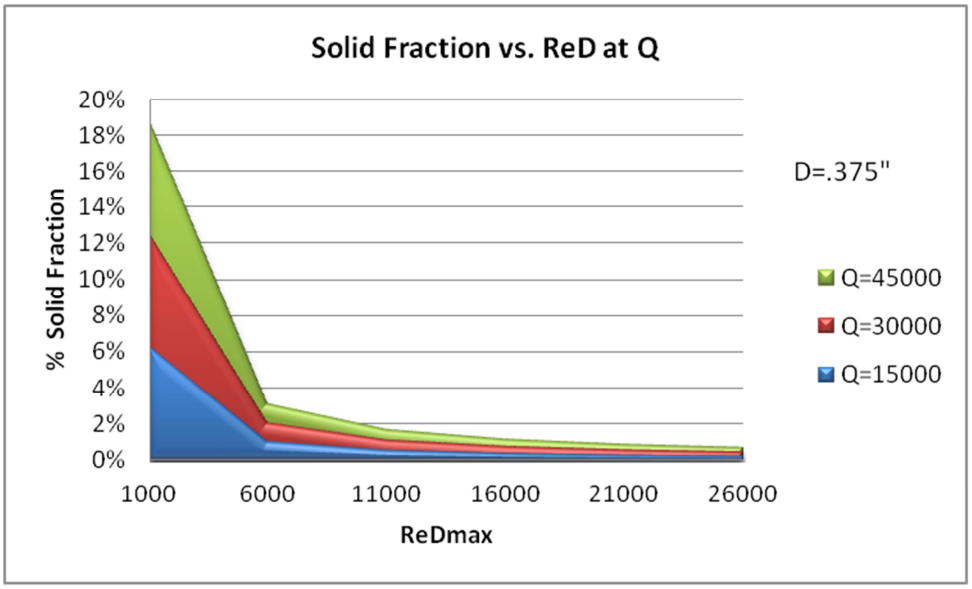

Figure 13: Solid Fraction at Reynolds at Different Heat Rates

Appendix 4.
Experiments with Laboratory Scale Prototype

Expected Outputs

Heat transfer coefficient (Ufreezesalt) as a function ofsolidification at near solification temperature
Heat transfer coefficient (Ufreezesalt) as a function of salt flow and heat transfer temperature difference

Heat transfer coeffieicent correlation from liquid molten salt

Pumpability of freezing mixture
Experience with handling high temperature molten salts near freezing point

Study Parameters	
Temperature of oil	various
Temperature of salt	high, medium, low
Flow rate of salt	high, low
Flow Rate of Oil	high, medium, low

Design of Experiment

Output	Oil Temperature, C	Oil Flow Rate	Salt temperature above freeze point	Salt Flow rate
liq to liq heat transfer coeff	320	high	high	high
liq to liq heat transfer coeff	320	medium	high	high
liq to liq heat transfer coeff	320	low	high	high
liq to liq heat transfer coeff	320	medium	high	low
liq to liq heat transfer coeff	311	low	high	low
solidification heat transfer coeff	311	medium	medium	low
solidification heat transfer coeff	305	medium	medium	low
solidification heat transfer coeff	300	medium	medium	low
solidification heat transfer coeff	280	medium	medium	low
solidification heat transfer coeff	270	medium	medium	low
solidification heat transfer coeff	260	medium	medium	low
solidification heat transfer coeff	260	medium	low	low
solidification heat transfer coeff	250	medium	low	high
solidification heat transfer coeff	250	medium	medium	low
solidification heat transfer coeff	320	medium	high	low
shut down mode	320	medium	heaters off	pump off
shut down mode	fan on	pump off	heaters off	pump off

Label (activity-date)	expt no.	What / Why	How	What should be observed and what data should be recorded Data	Experiment Parameters
Shakedown Tests					
Pre-20110202	1	Melting of Salt	Add using premelter and direct to tank	Time for initial melt of salt. Precautions during adding salt. Note all incidents. Record all temperatures	Salt addition rate. Mixing of salt.
Pre-201102xx	2	Salt Loop fidelity test and pump/ flow characteristics	Salt pump ON. Bypass heat exchanger. Pump salt through the loop; keep all heaters on. Salt temperature should be at least 25C above melting point	Record flow rate, pump speed, salt temperaturesand loop salt temps every 2 minutes. Record visual observations and interpretations in data book	Vary pump speed
Pre-201102xx	3	Salt Loop fidelity test and pump/ flow characteristics	Salt pump ON. Heat exchanger in loop. Pump salt through the loop; keep all heaters on. Salt temperature should be 25C above melting point	Record flow rate, pump speed, salt temperaturesand loop salt temps every 2 minutes. Record visual observations and interpretations in data book	Vary pump speed
Pre-201102xx	4	Therminol loop fidelity tests	Therminol pump ON. By pass heat exchanger.	Test for leaks and flow rate / pressure characteristics without Heat Exchanger	
Pre-201102xx	5	Therminol loop fidelity tests	Therminol pump ON. Salt Pump OFF With heat exchanger.	Test for leaks and flow rate / pressure characteristics without Heat Exchanger	
Pre-201102xx	6	Experiment loop fidelity	Both pumps ON with heat exchanger	Check heat exchanger for leaks or reactions with salt and oil (hope not). Confirm flow rates.	Keep temperatures of salt and therminol same about 350C or greater

Liquid Molten Salt (~350C) Heat Transfer Tests					
LMS-201102xx	7-x	Heat transfer for MOLTEN salt (liquid).		Record flow rates, temperature, pump power, pump speed, all data whatever available every minute. Observation records in excel notebook every 5 minutes.	Fixed salt temperature. pick 3 delta T and four flow rates for salt with therminol at ~90%but constant therminol flow. Vary delta T between therminol and salt temperature starting at expt 6 conditions and gradually reducing Temp. Vary salt flow rates
LMS-201102xx	8-x	Heat transfer for MOLTEN salt (liquid). Repeat 7 with different salt temp		Record flow rates, temperature, pump power, pump speed, all data whatever available every minute. Observation records in excel notebook every 5 minutes.	Approximately fixed salt temperature. pick 3 delta T and four flow rates for salt with therminol at ~90%but constant therminol flow. Vary delta T between therminol and salt temperature starting at expt 6 conditions and gradually reducing Temp. Vary salt flow rates
LMS-201102xx	9	Discover melting temperature	Gradually drop tmperatures everywhere till the salt temperature drops to near melting.	Observe pump flow charactierstics, heat transfer rates (coeff). (note: when you begin to see noticeable change then some freezing may be happening!)	

Appendix 5.
State-of-the-Art Power Tower System Analysis

Simulation Results for a Central Receiver and Energy Storage System

Gyan Hajela,
Pratt & Whitney Rocketdyne (PWR)

In order to properly perform system analyses and to perform trade studies, a computer program is developed to model the central receiver including the field of heliostats, the molten salt cooling loop to transfer energy from the receiver to the thermal storage tank and the phase change circulating loop.

A concentrated solar power (CSP) computer program is used to model the details of the field of heliostats and the central receiver. This includes the size of the field, number and size of heliostats, heliostat optical properties, heliostat locations, location of the field (latitude and longitude), field slope (if any), height of the receiver tower, diameter and the length of the receiver section, etc. This model is used to compute incident power on the receiver as a function of the time of the day and the day of the year.

A molten salt system (MSS) model is used to compute the energy absorbed by the circulating molten salt as it flows through the receiver panels and the energy transferred to the phase change fluid through the sensible heat exchanger, HX-3, and the latent heat exchanger, HX-4. This model will also compute pump power required to circulate the molten salt. The model will also perform detailed thermal, stress and strain calculations to ensure that the receiver panels and tubes can safely sustain the operating conditions.

A thermal storage tank (TST) model is used to perform to compute the energy received from the molten salt loop, energy transferred to the steam generation loop via the super-heater heat exchanger, HX-1, and the vaporizer heat exchanger, HX-2, and the amount of energy stored.

These three models are linked to each other so that their inputs and outputs are properly exchanged. The chained model is run in a time-marching fashion so that the system mass and energy balances can be performed over a period of several hours or days while satisfying load for the steam generator subsystem.

The CSP model can also be used to design the field of heliostats, perform optimization studies to establish critical parameters, such as diameter to length ratio of the receiver, height of receiver tower, heliostat focal lengths, field offset ratio, etc.

The MSS model will also provide parameters that are used design the heat exchangers, fluid pump and the piping system. The CSP and the MSS models are used to develop morning start-up and evening shut down procedures for the molten salt system. The molten salt loop can not circulate through the receiver when the solar incident power is very low or absent. These models will also be used to develop safety procedures in the event of circulating pump failure (to protect receiver tubes from getting too hot) and a cloud cover over the field of heliostats (molten salt freezing in the receiver tubes), etc.

The TST model provides parameters that are used to design heat exchangers (super-heater and the vaporizer), to size the storage tank , and the piping system.

The current scope of this model excludes the water system, though it may be added later on. At this stage the water system are modeled as a thermal load only.

Figure 1 shows the inputs and outputs for these models and how these models interface with each other.

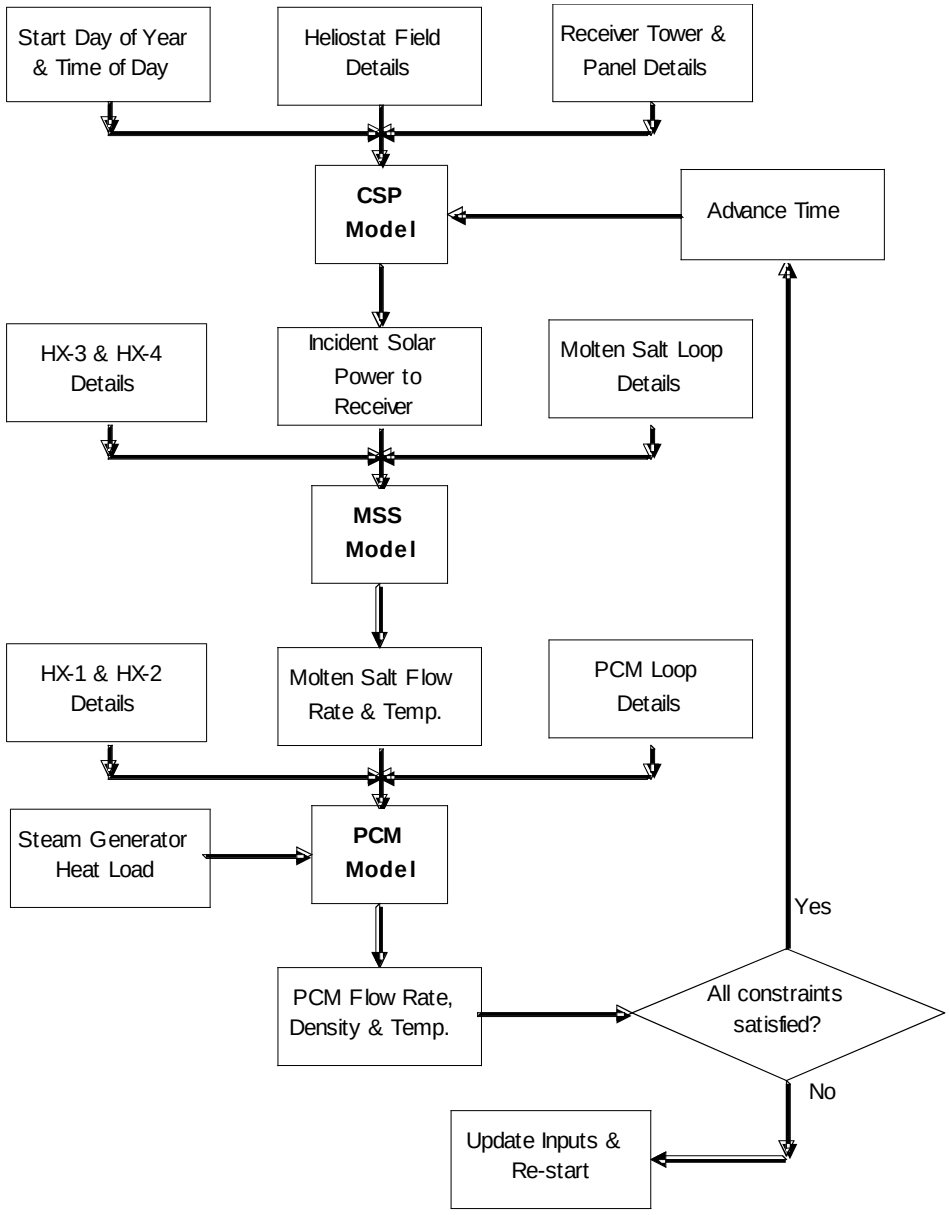

Figure 1. Model Process Diagram

Concentrated Solar Power Model Parameters

To demonstrate the process an existing model was used with the following inputs:

Field of Heliostats:		
Location		Cinco Casas
Latitude, deg	deg	39
Site elevation, km	km	0.65
Atmospheric visibility, km	km	23
Number of heliostats		17,170
Exclusion zone radius, m	m	122
Total land area available (circular field), km^2	sq km	6.3
Number of row of mirrors on heliostat		5
Number of columns of mirrors on heliostat		5
Effective vertical dimension of heliostat, m	m	7.35
Effective horizontal dimension of heliostat, m	m	8.5
Heliostats canted in x-axis		yes
Heliostats canted in y-axis		yes
Heliostat focal lengths, m	m	550, 1050 &
		1500
Average reflectivity of mirror surface		0.92
Standard deviation of the normal error distribution of		
elevation and azimuthal angles, mrad	mrad	1.5
Standard deviation of the normal error distribution of		
reflective surface in horizontal & vertical directions, mrad	mrad	1.5
Standard deviation of the normal error distribution caused		
by wind in horizontal and vertical directions, mrad	mrad	1.5

Receiver Tower:		
Height of the center of receiver above heliostat axis, m	m	175.5
Receiver effective height, m	m	18.3
Receiver effective diameter, m	m	15.1

For the configuration specified above, the solar incident power on the receiver is shown in Figure 2.

For the operation of the molten salt system, the day is the period when the sun elevation is greater than 15 degree above the horizon. Molten salt system flow rate is gradually started, in the morning, as the receiver panels start to heat and is shut down slowly, in the evening, as the incident power starts to drop.

The model can be applied to other site conditions and receiver designs.

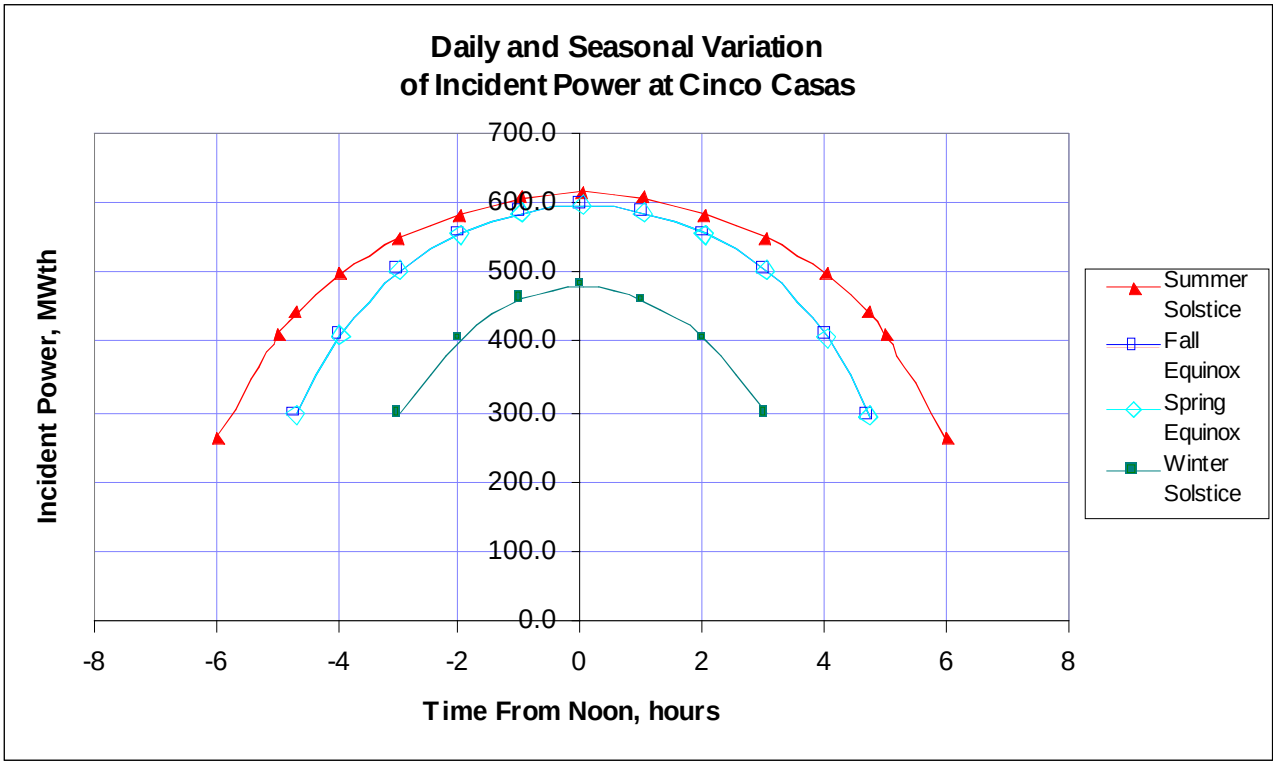

Figure 2. Incident Power Predictions

Heat Transfer Fluid (Low Melting Molten Salt) Subsystem Model Parameters

To demonstrate the process an existing model are used with the following design inputs:

Molten salt composition 60% $NaNO_3$ + 40% KNO_3
Salt temperature at receiver panel inlet, ˚C 288 (550 ˚F)
Salt temperature at receiver panel outlet, ˚C 566 (1050 ˚F)
Number of receiver panels 14
Number of flow circuits in the receiver 2
Panel height, m 18.3 (60 ft)
Panel width, m 3.35 (11 ft)
Ambient temperature around the receiver, ˚C 16 (60 ˚F)
Wind velocity, km/hr 18 (11 mph)
Panel surface reflectivity 0.060
Panel surface emissivity 0.89

For the configuration defined above, the molten salt flow rate is shown in Figure 3.

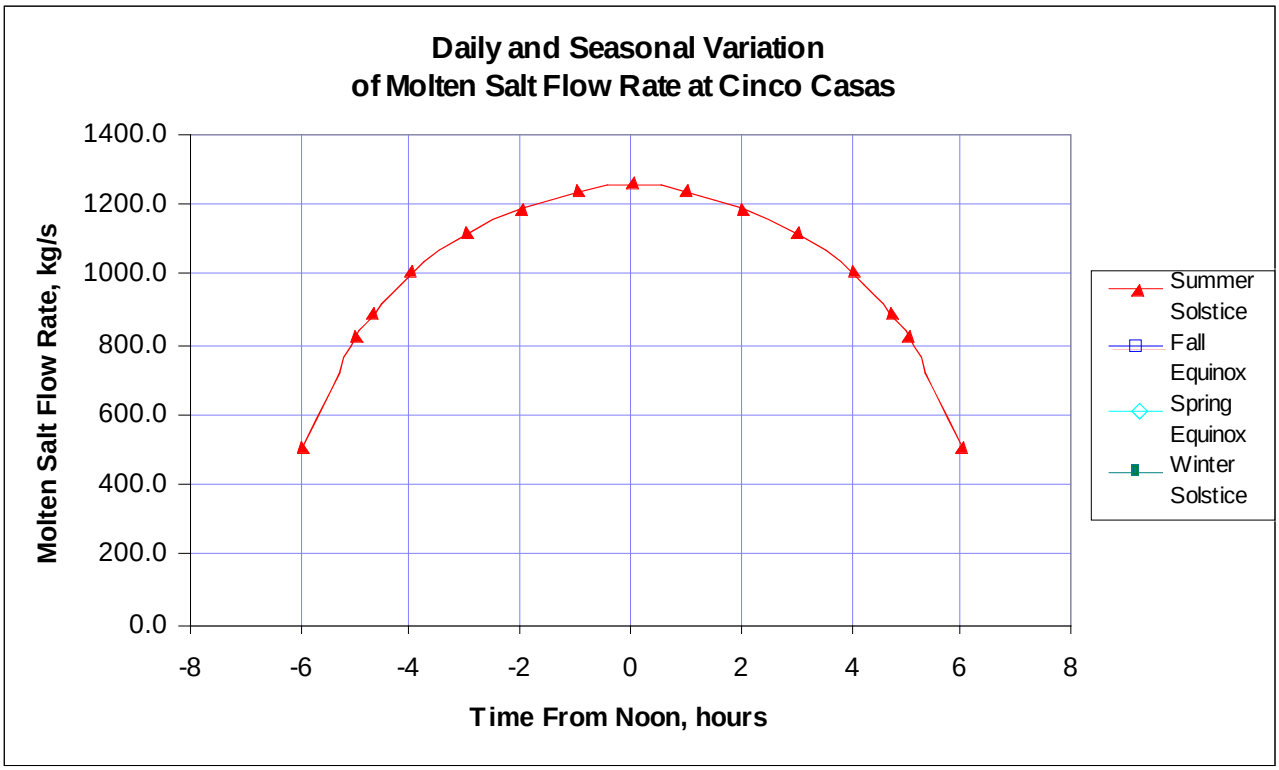

Figure 3. Molten Salt Flow Rate Predictions

Normal Operation

Normal operation is defined as an operation that enables molten salt outlet (from receiver) at the design value (1050 F) and molten salt flow rate greater than 20% of the rated flow rate. Molten salt flow rate can not be maintained at a value below 20% of the rated flow rate. The outlet temperature must be

maintained close to the design value to ensure that the PCM outlet temperature stays close to its design value, which, in turn, is essential to ensure that the superheated steam temperature stays close to its design value.

There are times when the operating conditions do not meet the criteria described above, such as, start-up, shut-down and transient cloud cover. During these conditions the HX-3 is bypassed and the receiver fluid is directed to bottom of tank heat exchanger HX-4 to melt the salt in the tank**.**

Special cases

The models describe above can be used to assess special cases. One such case is described and assessed below. These case provides a model for thermal efficiency as function of outlet temperature.

Case 1. Receiver Thermal Efficiency as a Function of HTF Outlet Temperature

The receiver absorbed the solar flux reflected to the receiver by the field of heliostats. The receiver performance may be defined as:

Receiver Thermal Efficiency = Heat Rate added to HTF molten salt / Incident solar power

Some of the incident solar power is lost by radiation and convection from the receiver panel surfaces. This heat loss is a function of receiver panel surface temperature. The panel surface temperature is directly controlled by the desired molten salt outlet temperature.

The molten salt model is run for a fixed day and time with different molten salt outlet temperatures. For this assessment, the molten salt model is run for the spring equinox (day 81) noon, when the incident power on the receiver was 597 MWth (Figure 4).

The model is run for three molten salt temperatures, 566, 510 and 454 ºC (1050, 950 and 850 ºF). The molten salt inlet temperature was fixed at 288 ºC (550 F). The receiver efficiency vs. molten salt outlet temperature is shown in the table below:

Outlet Temperature		Salt Flow Rate		Receiver
F	C	lb/s	kg/s	Efficiency, %
1050	566	2677	1217	85.9%
950	510	3392	1542	87.0%
850	454	4576	2080	88.0%

As expected, the receiver efficiency is reduced at higher operating temperatures.

Typical Solar Power Tower P/ T / F Fluid Conditions

Solar Thermal Power Plant

Heat Balance Data

#	Description		Case #1	Case #2
-	Ambient Conditions	Ambient DB Temperature (F)	110.0	
-	Ambient Conditions	Ambient WB Temperature (F)	70.0	
-	Ambient Conditions	Ambient WB Pressure (psia)	13.50	
-	System Performance	Gross Power Output (kW)	154,834	
-	System Performance	Aux Loads (kW)	4,966	
-	System Performance	Net Output (kW)	149,868	
-	System Performance	Steam Cycle Efficiency	38.2%	
1	Molten Salt from Hot Tank	Flow (lb/hr)		
		Temp (F)		
		Press (psia)		
		Enthalpy (BTU/lb)		
2	Hot Salt Pump Discharge	Flow (lb/hr)		
		Temp (F)		
		Press (psia)		
		Enthalpy (BTU/lb)		
3	Molten Salt to Superheater	Flow (lb/hr)		
		Temp (F)		
		Press (psia)		
		Enthalpy (BTU/lb)		
4	Molten Salt to Reheater	Flow (lb/hr)		
		Temp (F)		
		Press (psia)		
		Enthalpy (BTU/lb)		
5	Molten Salt from Superheater	Flow (lb/hr)		
		Temp (F)		
		Press (psia)		
		Enthalpy (BTU/lb)		
6	Molten Salt from Reheater	Flow (lb/hr)		
		Temp (F)		
		Press (psia)		
		Enthalpy (BTU/lb)		
7	Molten Salt Supply to Boiler	Flow (lb/hr)		
		Temp (F)		
		Press (psia)		
		Enthalpy (BTU/lb)		
8	Molten Salt to Economizer	Flow (lb/hr)		

		Temp (F)		
		Press (psia)		
		Enthalpy (BTU/lb)		
9	Molten Salt to IP Evaporator	Flow (lb/hr)		
		Temp (F)		
		Press (psia)		
		Enthalpy (BTU/lb)		
10	Molten Salt to Cold Tank	Flow (lb/hr)		
		Temp (F)		
		Press (psia)		
		Enthalpy (BTU/lb)		
11	HP Steam to STG	Flow (lb/hr)	1,093,894	
		Temp (F)	1,000	
		Press (psia)	1,813	
		Enthalpy (BTU/lb)	1,481	
12	CRH from STG	Flow (lb/hr)	1,093,894	
		Temp (F)	716	
		Press (psia)	590	
		Enthalpy (BTU/lb)	1,361	
13	CRH to Reheater	Flow (lb/hr)	1,093,894	
		Temp (F)	716	
		Press (psia)	590	
		Enthalpy (BTU/lb)	1,361	
14	HRH to STG	Flow (lb/hr)	1,093,894	
		Temp (F)	1,000	
		Press (psia)	578	
		Enthalpy (BTU/lb)	1,519	
15	IPT to LPT	Flow (lb/hr)	912,826	
		Temp (F)	558	
		Press (psia)	96	
		Enthalpy (BTU/lb)	1,309	
16	STG Exhaust	Flow (lb/hr)	810,715	
		Temp (F)	141	
		Press (psia)	3	
		Enthalpy (BTU/lb)	1,081	
17	Condenser Hotwell	Flow (lb/hr)	810,715	
		Temp (F)	135	
		Press (psia)	3	
		Enthalpy (BTU/lb)	103	
18	Condensate Pump Discharge to FWH1	Flow (lb/hr)	810,715	
		Temp (F)	135	
		Press (psia)	35	
		Enthalpy (BTU/lb)	103	
19	Condensate to FWH2	Flow (lb/hr)	864,850	
		Temp (F)	186	
		Press (psia)	35	

		Enthalpy (BTU/lb)	154	
20	Condensate to Deaerator	Flow (lb/hr)	864,850	
		Temp (F)	200	
		Press (psia)	34	
		Enthalpy (BTU/lb)	168	
21	Boiler Feed Pump Suction	Flow (lb/hr)	1,093,894	
		Temp (F)	257	
		Press (psia)	34	
		Enthalpy (BTU/lb)	226	
22	Feedwater to FWH3	Flow (lb/hr)	1,093,894	
		Temp (F)	261.1	
		Press (psia)	1,965.6	
		Enthalpy (BTU/lb)	233.9	
23	Feedwater to FWH4	Flow (lb/hr)	1,093,894	
		Temp (F)	351.5	
		Press (psia)	1,926.3	
		Enthalpy (BTU/lb)	326.1	
24	Feedwater to Economizer	Flow (lb/hr)	1,093,894	
		Temp (F)	446.3	
		Press (psia)	1,887.8	
		Enthalpy (BTU/lb)	427.0	
25	Economizer to Steam Drum	Flow (lb/hr)	1,093,894	
		Temp (F)	604.9	
		Press (psia)	1,850.0	
		Enthalpy (BTU/lb)	622.4	
26	Steam Drum to Recirc Pump	Flow (lb/hr)	1,455,649	
		Temp (F)	624.9	
		Press (psia)	1,850.0	
		Enthalpy (BTU/lb)	654.2	
27	Recirc Pump to Boiler	Flow (lb/hr)	1,455,649	
		Temp (F)	625.9	
		Press (psia)	1,887.8	
		Enthalpy (BTU/lb)	655.5	
28	Boiler to Steam Drum	Flow (lb/hr)	1,455,649	
		Temp (F)	624.9	
		Press (psia)	1,850.0	
		Enthalpy (BTU/lb)	1,048.7	
29	HP Steam to Superheater	Flow (lb/hr)	1,093,894	
		Temp (F)	624.9	
		Press (psia)	1,850.0	
		Enthalpy (BTU/lb)	1,147.3	
30	Feedwater to Throttle Valve	Flow (lb/hr)	0	
		Temp (F)	261.1	
		Press (psia)	1,965.6	
		Enthalpy (BTU/lb)	233.9	

31	Feedwater to IP Evaporator	Flow (lb/hr)	0	
		Temp (F)	263.9	
		Press (psia)	590.3	
		Enthalpy (BTU/lb)	233.9	
32	IP Steam to Reheater	Flow (lb/hr)	0	
		Temp (F)	263.9	
		Press (psia)	590.3	
		Enthalpy (BTU/lb)	233.9	
33	IP Extraction Steam to FWH4	Flow (lb/hr)	97,382	
		Temp (F)	913.6	
		Press (psia)	415.0	
		Enthalpy (BTU/lb)	1,477.1	
34	IP Extraction Steam to FWH3	Flow (lb/hr)	83,686	
		Temp (F)	642.0	
		Press (psia)	140.0	
		Enthalpy (BTU/lb)	1,347.9	
35	LP Extraction Steam to Deaerator	Flow (lb/hr)	47,976	
		Temp (F)	366.5	
		Press (psia)	34.6	
		Enthalpy (BTU/lb)	1,221.0	
36	LP Steam Extraction to FWH2	Flow (lb/hr)	11,658	
		Temp (F)	311.5	
		Press (psia)	25.0	
		Enthalpy (BTU/lb)	1,196.0	
37	LP Steam Extraction to FWH1	Flow (lb/hr)	42,477	
		Temp (F)	195.5	
		Press (psia)	10.5	
		Enthalpy (BTU/lb)	1,136.9	
38	Drain from FWH4	Flow (lb/hr)	97,382	
		Temp (F)	360.5	
		Press (psia)	406.7	
		Enthalpy (BTU/lb)	333.2	
39	Drain from FWH3	Flow (lb/hr)	181,068	
		Temp (F)	270.1	
		Press (psia)	137.2	
		Enthalpy (BTU/lb)	239.3	
40	Drain from FWH2	Flow (lb/hr)	11,658	
		Temp (F)	195.1	
		Press (psia)	11.5	
		Enthalpy (BTU/lb)	163.2	
41	Drain from FWH1	Flow (lb/hr)	54,135	
		Temp (F)	144.1	
		Press (psia)	10.3	
		Enthalpy (BTU/lb)	112.0	
42	FWH1 Drain Pump Discharge	Flow (lb/hr)	54,135	

		Temp (F)	144.1	
		Press (psia)	34.5	
		Enthalpy (BTU/lb)	112.1	
43	Cooling Water to Condensor	Flow (lb/hr)	39,748,338	
		Temp (F)	116.3	
		Press (psia)	25.0	
		Enthalpy (BTU/lb)	84.4	
44	Cooling Water to Cooling Tower	Flow (lb/hr)	39,748,338	
		Temp (F)	136.3	
		Press (psia)	15.1	
		Enthalpy (BTU/lb)	104.4	
45	Cooling Water to Cooling Water Pump	Flow (lb/hr)	39,748,338	
		Temp (F)	116.3	
		Press (psia)	14.8	
		Enthalpy (BTU/lb)	84.4	